LOW WAVE NUMBER LEVELS OF TURBULENT BOUNDARY LAYER WALL PRESSURE FLUCTUATIONS IN ZERO AND ADVERSE GRADIENTS

by
M. Moeller
P. Leehey
N. C. Martin

Report No. 82464-2

September 1978

This research was carried out under the sponsorship of the Sensor Technology Program, Code 222, Office of Naval Research, Contract No. N00014-75-C-0509.

ACOUSTICS AND VIBRATION LABORATORY
Massachusetts Institute of Technology
Cambridge, Massachusetts 02139

LEVEL II

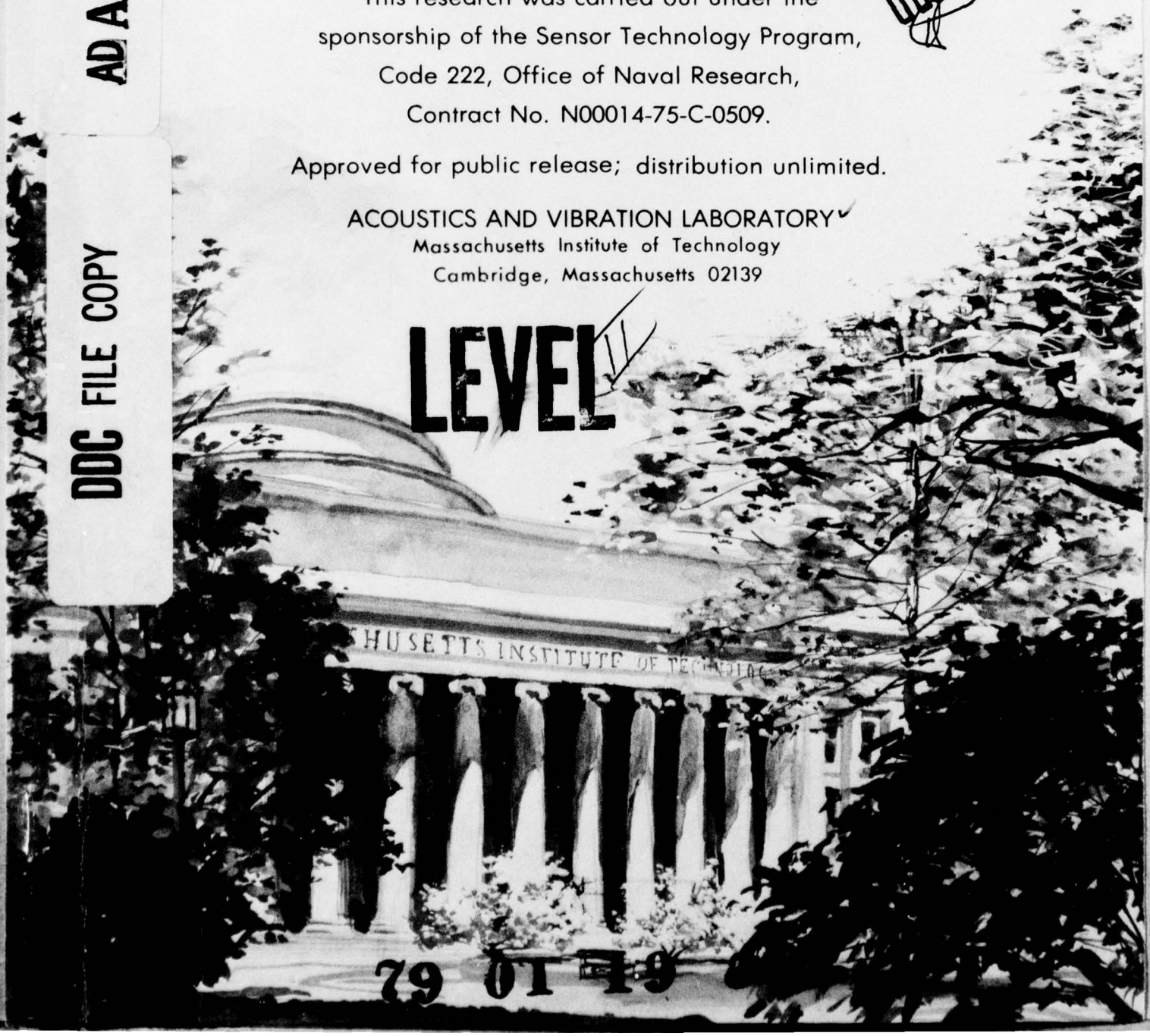

LOW WAVENUMBER LEVELS OF TURBULENT BOUNDARY LAYER WALL PRESSURE FLUCTUATIONS IN ZERO AND ADVERSE GRADIENTS

by

M. Moeller
P. Leehey
N. C. Martin

Report No. 82464-2

September 1978

This research was carried out under
the sponsorship of the Sensor Technology Program,
Code 222, Office of Naval Research,
Contract No. N00014-75-C-0509

Acoustics and Vibration Laboratory
Massachusetts Institute of Technology
Cambridge, Massachusetts 02139

SECURITY CLASSIFICATION OF THIS PAGE (When Data Entered)

REPORT DOCUMENTATION PAGE	READ INSTRUCTIONS BEFORE COMPLETING FORM
1. REPORT NUMBER AV-Acoustics & Vibration Lab. 82464-2	2. GOVT ACCESSION NO.
	3. RECIPIENT'S CATALOG NUMBER Rept.
4. TITLE (and Subtitle) Low Wavenumber Levels of Turbulent Boundary Layer Wall Pressure Fluctuations in Zero and Adverse Gradients.	5. TYPE OF REPORT & PERIOD COVERED Final March 1976 Through September 1977
	6. PERFORMING ORG. REPORT NUMBER
7. AUTHOR(s) M. Moeller, P. Leehey and N.C. Martin	8. CONTRACT OR GRANT NUMBER(s) ONR-N00014-75-C-0509
9. PERFORMING ORGANIZATION NAME AND ADDRESS Massachusetts Institute of Technology Cambridge, Massachusetts 02139	10. PROGRAM ELEMENT, PROJECT, TASK AREA & WORK UNIT NUMBERS
11. CONTROLLING OFFICE NAME AND ADDRESS Sensor Technology Program Office of Naval Research Arlington, Virginia 22217	12. REPORT DATE September 1978
	13. NUMBER OF PAGES
14. MONITORING AGENCY NAME & ADDRESS (if different from Controlling Office) 87 p.	15. SECURITY CLASS. (of this report) Unclassified
	15a. DECLASSIFICATION/DOWNGRADING SCHEDULE

16. DISTRIBUTION STATEMENT (of this Report)

Approved for public release; distribution unlimited

17. DISTRIBUTION STATEMENT (of the abstract entered in Block 20, if different from Report)

18. SUPPLEMENTARY NOTES

19. KEY WORDS (Continue on reverse side if necessary and identify by block number)

Turbulent Boundary Layers
Low Wavenumber Levels
Flow Induced Vibration

20. ABSTRACT (Continue on reverse side if necessary and identify by block number)

The low wavenumber components of the turbulent boundary layer wavenumber frequency spectrum of wall pressure fluctuations were measured with two flush-mounted rectangular plates with approximately clamped boundary conditions. The plates were designed to provide low wavenumber measurements at higher frequencies and wave numbers than previous plate experiments in order to provide data comparable with measurements made by Farabee and Geib [7]

DD FORM 1 JAN 73 1473 EDITION OF 1 NOV 65 IS OBSOLETE S/N 0102-014-6601

405 028

using an array of flush mounted microphones. The low wavenumber measurements were made in the M.I.T. low noise low turbulence subsonic wind tunnel under zero and adverse pressure gradient conditions. When nondimensionalized on outer boundary layer variables the adverse pressure gradient data do not exhibit increased levels from those of the zero pressure gradient data. The zero pressure gradient data are in good agreement with the levels reported by Farabee & Geib [7] for the same nondimensional frequency and wavenumber range.

LOW WAVENUMBER LEVELS OF TURBULENT BOUNDARY LAYER WALL PRESSURE FLUCTUATIONS IN ZERO AND ADVERSE GRADIENTS

by

M. Moeller, P. Leehey, and N. C. Martin

ABSTRACT

The low wavenumber components of the turbulent boundary layer wavenumber frequency spectrum of wall pressure fluctuations were measured with two flush-mounted rectangular plates having approximately clamped boundary conditions. The plates were designed to provide low wavenumber measurements at higher frequencies and wavenumbers than previous plate experiments in order to provide data comparable with measurements made by Farabee and Geib [7] with an array of flush-mounted microphones. The low wavenumber measurements were made in the M.I.T. low noise low turbulence subsonic wind tunnel under zero and adverse pressure gradient conditions. When nondimensionalized on outer boundary layer variables the adverse pressure gradient data do not exhibit increased levels from those of the zero pressure gradient data. The zero pressure gradient data are in good agreement with the levels reported by Farabee and Geib [7] for the same nondimensional frequency and wavenumber range.

TABLE OF CONTENTS

LIST OF TABLES

LIST OF FIGURES

Figure No.

LIST OF SYMBOLS

$A_m(k_1)$	Longitudinal (Streamwise) shape factor
$A_n(k_3)$	Lateral shape factor
$\|A_m(k_1)\|^2$	Longitudinal (streamwise) wavenumber filter shape function
$\|A_n(k_3)\|^2$	Lateral wavenumber filter shape function
c_o	Velocity of sound in air
D	Flexural rigidity
$f_{mn}(x,z)$	Two-dimensional mode shape of the (m,n) mode
f_{mn}	Natural (cyclic) frequency of the (m,n) mode
Δf_{mn}	Equivalent rectangular bandwidth of the (m,n) mode
$\|F_{mn}(k_1,k_3)\|^2$	Two-dimensional wavenumber filter shape function
$g_m(x)$	Longitudinal mode shape
$h_n(z)$	Lateral mode shape
H	Boundary layer shape factor, $H=\delta^*/\theta$
$k=\|\vec{K}\|$	Wavenumber: k_1, longitudinal; k_3, lateral
k_a	Acoustic wavenumber, $k_a=\omega/c_o$
k_c	Convective wavenumber, $k_c=\omega/U_c$
k^*	Nondimensional wavenumber, $k^*=k\ \delta^*$
$\Delta\bar{k}_e$	Equivalent rectangular bandwidth of $\|A_m(k_1)\|^2$
L	Structural dimension: L_1, longitudinal; L_3, lateral
$P(k_1,k_3,\omega)$	Measured wavenumber frequency spectral density of wall pressure

q	Free stream dynamic pressure, $q=\frac{1}{2}\rho U_\infty^2$
r	Measurement separation distance: r_1, longitudinal; r_3, lateral
$S_a(x,z,\omega)$	Theoretical acceleration spectral density, $-\infty<\omega<\infty$
$\hat{S}_a(x,z,f)$	Experimental acceleration spectral density, $o<f<\infty$
U_c	Convection velocity
U_∞	Free stream velocity
U_τ	Friction velocity
x	Longitudinal distance variable
z	Lateral distance variable
δ^*	Boundary layer displacement thickness
η	Damping loss factor, equivalent to twice the fraction of critical damping
θ	Boundary layer momentum thickness
ρ	Fluid density
σ	Structural surface density
$\Phi_A(\omega)$	Theoretical spectral density of acoustic pressure fluctuations, $-\infty<\omega<\infty$
$\hat{\Phi}_A(f)$	Experimental spectral density of acoustic pressure fluctuations, $o<f<\infty$, $\hat{\Phi}_A(f) = 4\pi\Phi_A(\omega)$
$\Phi_p(\omega)$	Theoretical spectral density of single point wall pressure fluctuations, $-\infty<\omega<\infty$
$\Phi_p(k_1,k_3,\omega)$	Theoretical wavenumber-frequency spectral density of wall pressure, $-\infty<\omega<\infty$
$\Phi_c(k_1,k_3,\omega)$	Convective model of $\Phi_p(k_1,k_3,\omega)$

$\Phi_p(r_1,r_3,\omega)$	Theoretical cross spectral density of wall pressure
ω	Angular frequency, $\omega = 2\pi f$
ω_{mn}	Angular resonance frequency of (m,n) mode
ω^*	Nondimensional frequency, $\omega^*=\omega\delta^*/U_\infty$

1. INTRODUCTION

Structural vibration induced by the wall pressure fluctuations beneath a turbulent boundary layer is an area of concern in marine and aircraft structures. This paper is primarily concerned with marine structures.

The wall pressure fluctuation beneath a turbulent boundary layer is a random phenomenon and it is necessary to describe it statistically. In the case of zero freestream pressure gradient, the boundary layer can be assumed time-stationary and spatially homogeneous. With these assumptions, the wall pressure can be described by its cross-spectral density, $\Phi_p(r_1,r_3,\omega)$. The wall pressure can also be described by its wavenumber-frequency spectrum, $\Phi_p(k_1,k_3,\omega)$. The wavenumber-frequency spectrum is the Fourier transform of the cross-spectral density, and is defined by

$$\Phi_p(k_1,k_3,\omega) = \frac{1}{(2\pi)^2} \int_{-\infty}^{\infty} \int \Phi_p(r_1,r_3,\omega) e^{i(k_1 r_1 + k_3 r_3)} dr_1 dr_3 \qquad (1.1)$$

The behavior of the wavenumber-frequency spectrum is governed by the decay and convection of eddies in the turbulent boundary layer. The convection of eddies leads to high values of the wavenumber-frequency spectrum along a convective ridge defined by $k_c = \omega/U_c(\omega)$, where $U_c(\omega)$ is the convection velocity, which is a function of frequency.

In most marine applications the frequencies of interest are relatively high and the freestream velocity is low. As a result of this the convected pressure disturbances have a spatial scale much smaller than the wavelength of the free bending waves of most marine structures and are therefore inefficient at producing structural vibration. Sources of excitation better coupled to the free bending waves of most marine structures are the low wavenumber (i.e., large wavelength) components of the turbulent boundary layer wall pressure spectrum.

The wall pressure spectrum of a turbulent boundary layer is dominated by the convective pressure fluctuations. Cross-spectral density measurements of the convective ridge have been made by various experimenters using pairs of flush-mounted pressure transducers. Some investigators who have used this technique are Blake [1] and Burton [2]. Wills [3] took cross-spectral density data and then transformed them into wavenumber frequency space. Unfortunately, the low wavenumber components do not contribute significantly to the single point wall pressure spectrum. Because of the extremely low levels of the low wavenumber components of the turbulent boundary layer, it is necessary to construct spatial filters to measure them. Maidanik and Jorgensen [4] have demonstrated that an array of flush-mounted pressure transducers can be used as a spatial filter. Blake and Chase [5], Jameson [6], and Farabee and

Geib [7] have used this method to measure the low wavenumber levels of a turbulent boundary layer. Another approach is to utilize the spatial filtering characteristics of continuous mechanical strurctures. Aupperle and Lambert [8] described analytically how a beam could be used as a spatial filter. Martin and Leehey [9] used a membrane, and Jameson [10] and Martin [11] used plates as spatial filters.

Up to this point in time the use of plates as spatial filters and the use of microphone arrays have yielded data in different ranges of nondimensional frequency ω^*, where $\omega^* = \omega\delta^*/U_\infty$ (δ^* is the displacement thickness of the boundary layer and U_∞ is the freestream velocity). Figure (1.1) shows the existing data as a function of nondimensional frequency. The data of Martin [11], Martin and Leehey [9], and Jameson [10] taken using plates and membranes were in the nondimensional frequency range of $0.8 < \omega\delta^*/U_\infty < 4.0$. The microphone array data of Farabee and Geib [5] were in the ranges $5.0 < \omega\delta^*/U_\infty < 10.0$ and $10.0 < \omega\delta^*/U_\infty < 30.0$; there was some concern about the data in the range $5.0 < \omega\delta^*/U_\infty < 10.0$ being contaminated by either acoustic or convective contamination. The zero-gradient work in this paper was carried out to provide a region of direct comparison between microphone array data and data taken using the spatial filtering characteristics of plates. The experimental technique used in this paper was to utilize

the spatial filtering of fully clamped plates. The nondimensional frequency range of interest was $5.0 < \omega\delta^*/U_\infty < 10.0$. Two new wavenumber filters were designed and constructed and then used to measure the low wavenumber levels in the region $5.0 < \omega\delta^*/U_\infty < 10.0$.

The effect of flow inhomogeneity on the low wavenumber levels of a turbulent boundary layer was also investigated. The flow inhomogeneity was accomplished by imposing an adverse pressure gradient on the mean flow. In the region of the adverse gradient the boundary layer was rapidly thickening towards separation and so the inhomogeneity was quite severe.

Over what ranges of the variables the low-wavenumber levels can be presented, approximately, in terms of just the outer or just the inner boundary-layer parameters is not yet evident. Measuring the low wavenumber levels of the adverse gradient boundary layer may provide some information because the mean wall shear stress was greatly reduced by the adverse gradient and so there was a significant variation of the inner flow parameters. Similarly the adverse gradient significantly increases the boundary layer thickness so that outer parameter scalings will also be changed. However, the adverse gradient also introduces an inhomogeneity in the flow field (i.e.: the boundary layer thickness and wall shear stress are changing rapidly in the downstream direction). Thus, it may be

difficult to distinguish between effects resulting from the variations in inner or outer parameters and the effects of the flow inhomogeneity.

2. THE RESPONSE OF A PLATE TO A RANDOM PRESSURE FIELD

In this chapter the response of a plate to a normal random pressure field is reviewed. Only the results pertinent to this study are presented; a detailed derivation can be found in "Wavenumber Filtering by Mechanical Structures" by N. C. Martin [11].

2.1 Plate Response

The plates are characterized by dimensions L_1 and L_3, by a uniform mass per unit area, σ, and by their flexural rigidity, D. The modal damping factor, η_{mn}, is the total damping of the plate including both radiation damping and structural damping.

For the undamped free vibration of a plate, there exist a set of normal modes, $f_{mn}(x,z)$, with eigenvalues, ω_{mn}, which satisfy the governing partial differential equation subject to the appropriate boundary conditions. In many cases the normal mode shape, $f_{mn}(x,z)$ can be separated into an x-dependent term and a z-dependent term. For clamped plates this does not yield an exact solution, but the use of clamped beam functions as mode shapes is a reasonable approximation. The mode shape of the plates is therefore expressed in separable form as

$$f_{mn}(x,z) = g_m(x)\ h_n\ (z). \tag{2.1}$$

The two-dimensional spatial transform of the normal mode shape is defined by

$$F_{mn}(k_1,k_3) = \int_o^{L_1} \int_o^{L_3} f_{mn}(x,z) e^{i(k_1 x + k_3 z)} \, dx \, dz \tag{2.2}$$

Using Equation (2.1) one can define one-dimensional spatial transforms as:

$$A_m(k_1) = \int_o^{L_1} g_m(x) \, e^{ik_1 x} \, dx \tag{2.3a}$$

$$A_n(k_3) = \int_o^{L_3} h_n(z) \, e^{ik_3 z} \, dz. \tag{2.3b}$$

Note that the normalization of the mode shapes is here defined as:

$$\int_o^{L_1} \int_o^{L_3} f_{mn}(x,z) \, f_{jk}(x,z) \, dx \, dz = \delta_{mj} \, \delta_{nk}$$

where δ_{mj} is the Kronecker delta function. As a result the one-dimensional mode shapes $h_n(z)$ and $g_m(x)$ have dimensions of $L_3^{-1/2}$ and $L_1^{-1/2}$, respectively. The transforms $A_n(k_3)$ and $A_m(k_1)$ thus have dimensions of $L_3^{1/2}$ and $L_1^{1/2}$, respectively.

The wavenumber filter shape, $|F_{mn}(k_1,k_3)|^2$, is the squared magnitude of the two-dimensional spatial transform of the normal mode shape defined in Equation (2.2). This wavenumber filter shape can now be expressed in terms of the one-dimensional wavenumber filter shapes,

$$|F_{mn}(k_1,k_3)|^2 = |A_m(k_1)|^2 \; |A_n(k_3)|^2. \tag{2.4}$$

The wavenumber filter shape is a modal characteristic and is different for each mode. Since the mode shape depends on the boundary conditions of the plate, so does the wavenumber filter shape. The wavenumber filter shape is important in determining the plate response to a random pressure field.

The acceleration spectral density of the plate, $S_a(x,z,\omega_{mn})$, can be expressed in terms of the wavenumber frequency spectrum of the turbulent boundary layer $\Phi_p(k_1,k_3,\omega)$; the wavenumber filter shape, $|F_{mn}(k_1,k_3)|^2$; the normal mode shape, $f_{mn}(x,z)$; the modal frequency, ω_{mn}; the modal damping factor, η_{mn}; and the modal mass, σ_{mn}. The result is (see Martin [11]).

$$S_a(x,z,\omega_{mn}) = \frac{f_{mn}^2(x,z)}{(\sigma\eta)_{mn}^2} \int_{-\infty}^{\infty} \int_{-\infty}^{\infty} |F_{mn}(k_1,k_3)|^2 \Phi_p(k_1,k_3,\omega_{mn})\, dk_1 dk_3 \tag{2.5}$$

This equation is valid only at the resonant frequencies of the plate. It is significant to note that all that is required to evaluate this expression are the modal mass, the modal damping, and the modal frequency, all of which can be experimentally determined, and the wavenumber filter shape, which is determined analytically from clamped beam mode shapes.

2.2 Sources of Excitation

The plate in the wind tunnel responds to the low wavenumber levels, to the convective ridge, and also to the acoustic background noise. Figure (2.1) is a schematic of the variation of magnitude of the wavenumber-frequency spectrum at a particular frequency as a function of streamwise wavenumber. From Figure (2.1) it can be seen that there is a great deal of energy in the convective ridge region. The wavenumber filter shape must therefore discriminate against high wavenumber excitation. Also it is important that the wavenumber filter shape discriminate against acoustic excitation.

A sample wavenumber filter shape is plotted in Figure (2.2). The wavenumber filter shape is symmetric in k_1 and so is plotted only for $k_1 \geq 0$. The wavenumber filter shape is characterized by major lobes centered at $k_1 = \pm k_m$, $k_m \simeq (m + 1/2)\ \pi/L_1$. The side lobes of the wavenumber filter shape determine how the plate will respond to excitation at lower, $k_1 < k_m$, and higher, $k_1 > k_m$, wavenumbers. For a fully clamped plate the high wavenumber behavior goes as $1/k_1^6$, so the greater the separation of the modal wavenumber from the convective ridge, the lower the convective contaminating levels. This is also true to some extent for separation in wavenumber between the modal wavenumber and acoustic

wavenumber, $k_1 = \omega/c_o$. Figure (2.3) illustrates the location of the modes in wavenumber-frequency space. The frequency and wavenumber parameters have been non-dimensionalized on outer boundary layer parameters; δ^*, displacement thickness; and U_∞, the freestream velocity, so that

$$\omega^* = \omega\delta^*/U_\infty \tag{2.6a}$$

$$k_1^* = k_1\delta^* \tag{2.6b}$$

The low wavenumber region lies well below the convective ridge region, $k_1 = \omega/U_c(\omega)$ and above the acoustic region, $k = \omega/c_o$.

The plate responds to three separate sources of excitation. It is reasonable to assume that they are statistically independent and that the wavenumber-frequency spectrum can be described as an incoherent sum of the three sources: low wavenumber, acoustic, and convective ridge. Hence,

$$\Phi_p(k_1,k_3,\omega) = \Phi_{p_{low\ k}}(k_1,k_3,\omega) + \Phi_{p_{acoustic}}(k_1,k_3,\omega) + \Phi_{p_{conv.}}(k_1,k_3,\omega) \tag{2.7}$$

Equation (2.5) can be used to evaluate the contribution of the three separate sources of excitation. Careful evaluation of the contaminating levels is important to guarantee that the low wavenumber levels are actually measured.

2.3 Structural Response to Low Wavenumber Excitation

The plates were used as sensing devices to measure the low wavenumber levels of the turbulent boundary layer. The plate acceleration spectral density was measured at the center of the plates. Because the acceleration response was measured at the center of the plate, only the odd-odd modes were measured. Any even mode would have a node at the center of plate. In particular, the useful modes of the plate were the n=1, m odd modes. The lateral wavenumber filter shape of interest is for n=1, and is symmetric about k_3=0. The longitudinal wavenumber filter shapes of interest are for the m odd modes. These filter shapes are characterized by the major lobes centered at $k_1 = \pm k_m$ where $k_m \simeq (m + 1/2)\ \pi/L_1$.

If the excitation $\Phi_p(k_1,k_3,\omega)$ is reasonably constant with respect to k_1,k_3 in the low wavenumber region, then the integral of equation (2.5) will be dominated by the major lobes of the wavenumber filter shape. The wavenumber bandwidths of the wavenumber filter shape are narrow enough to allow an approximation of the wavenumber filter shape by Dirac delta functions at $k_3 = 0$ and $k_1 = \pm k_m$. The result is

$$|A_n(k_3)|^2 = 2\pi\ \delta(k_3) \tag{2.8a}$$

$$|A_m(k_1)|^2 = \pi[\delta(k_1 + k_m) + \delta(k_1 - k_m)] \tag{2.8b}$$

The substitution of equations (2.8) into (2.5) yields

$$S_a(x,z,\omega_{mn}) = \frac{2\pi^2\ f_{mn}^2(x,z)}{(\sigma\eta)_{mn}^2}[\Phi_p(k_m,0,\omega_{mn}) + \Phi_p(-k_m,0,\omega_{mn})] \tag{2.9}$$

Since the measured acceleration spectral response was made at the center of the plate, the quantity $f_{mn}^2(L_1/2,\ L_3/2,\omega_{mn})$ needs to be calculated from the odd clamped beam mode shapes. The result is

$$f_{mn}^2\left(\frac{L_1}{2},\ \frac{L_3}{2},\ \omega_{mn}\right) \simeq \frac{5.044}{L_1\ L_3}. \tag{2.10}$$

The acceleration spectral response in equation (2.9) includes terms of both $\Phi_p(k_m,0,\omega_{mn})$ and $\Phi_p(-k_m,0,\omega_{mn})$. Unfortunately, it is not possible to separate the two. On physical grounds, it is likely that $\Phi_p(-k_m,0,\omega_{mn}) << \Phi_p(k_m,0,\omega_{mn})$ for $k_1\delta^*$ sufficiently large. Both terms will be retained by defining

$$P(k_m,0,\omega_{mn}) = \Phi_p(k_m,0,\omega_{mn}) + \Phi_p(-k_m,0,\omega_{mn}). \tag{2.11}$$

Using equations (2.11), (2.10) and (2.9), the low wavenumber levels can be expressed by

$$P(k_m,0,\omega_{mn}) = \frac{L_1 L_3}{10.09\pi^2} (\sigma\eta)^2_{mn} S_a\left(\frac{L_1}{2}, \frac{L_3}{2}, \omega_{mn}\right). \qquad (2.12)$$

2.4 Structural Response to Convective Excitation

To estimate the response of the plate to convective excitation, it is necessary to have a model of the convective wavenumber-frequency spectrum. A model for this purpose was constructed by Martin [11]. The similarity form assumed for $\Phi_p(r_1,r_3,\omega)$ was

$$\Phi_p(r_1,r_3,\omega) = \Phi_p(\omega) \cdot A\left(\frac{\omega r_1}{U_c}\right) \cdot B\left(\frac{\omega r_3}{U_\infty}\right) e^{-i\omega r_1/U_c} \qquad (2.13)$$

Blake's data [10] were fitted to this similarity form with exponentials and then transformed analytically to wavenumber-frequency space by using equation (1.1). The model used by Martin [11] to estimate the convective contamination of the plate is

$$\text{A.} \quad \text{For } |k_3| \leq \Delta k_3 = \frac{.6\pi\omega}{U_\infty}$$

$$\Phi_c(k_1,k_3,\omega) = .728\, \Phi_p(\omega) \left(\frac{U_c U}{\omega^2}\right) \exp\left[-23.7\left(\frac{k_1 U_c}{\omega} - 1\right)^2\right]$$

$$\text{B.} \quad \text{For } |k_3| > \Delta k_3 = \frac{.6\pi\omega}{U_\infty} \qquad (2.14)$$

$$\Phi_c(k_1,k_3,\omega) = 0.$$

equation (2.14) can now be used with equation (2.5) to calculate a plate displacement spectral response. The clamped plate acceleration response is

$$S_a\left(\frac{L_1}{2}, \frac{L_3}{2}, \omega_{mn}\right)_{conv.} = 115.5 \left(\frac{U_\infty}{\omega_{mn} L_3}\right) \left(\frac{k_m^4}{k_c^6}\right) \left(\frac{\Phi_p(\omega_{mn})}{(\sigma\eta)_{mn}^2}\right) \quad (2.15)$$

2.5 Plate Response to Acoustic Excitation

To evaluate possible acoustic contamination, a model based on the measured acoustic spectrum in the wind tunnel was developed. The model is conservative because it assumes the acoustic field is concentrated at its highest wavenumber instead of spread out in wavenumber. The plates are acoustically slow so that the plate response is governed by the lower side lobes of the wavenumber filter shape. Since in reality a spread of wavenumbers is encountered, an average value of the wavenumber filter shape in the vicinity of ω/c_o is used in equation (2.5) to calculate the plate response due to the acoustic levels. From Martin [11], the result for a fully clamped plate is

$$S_a\left(\frac{L_1}{2}, \frac{L_3}{2}, \omega_{mn}\right)_{acoustic} = 27.9 \frac{\bar{k}_m^2 + \bar{k}_A^2}{1 - \bar{k}_m^{-1}} \left[\frac{\bar{k}_m^2}{\bar{k}_m^4 - \bar{k}_A^4}\right]^2 \frac{\Phi_A(\omega_{mn})}{(\sigma\eta)_{mn}^2} \quad (2.16)$$

with $\bar{k}_m = (m + 1/2)\,\pi$ and $\bar{k}_A = \omega_{mn} L_1/c_o$.

3. THE EXPERIMENTAL FACILITY AND PROGRAMS

The last chapter related the low wavenumber levels of a turbulent boundary layer to the acceleration spectral response of a plate. In this chapter the experimental facility, the design of the new wavenumber filters, and the measurement programs are described.

3.1 The Experimental Facility

The experiments were conducted in the M.I.T. low-noise, low-turbulence wind tunnel using the equipment of the M.I.T. Acoustic and Vibration Laboratory. A detailed description of this facility has been given by Hanson [12], and it is shown in Figure (3.1). The wind tunnel consists of an intake, a flow straightening and settling chamber, a contraction, a test section enclosed in an airtight blockhouse, a muffler diffuser, and a variable speed centrifugal blower.

Boundary layer properties have been measured in this facility by Blake [1] and by Burton [2]. Martin and Leehey [9] and Martin [11] used this facility for their low wavenumber measurements. The wind tunnel has been modified since their work was completed. The settling chamber was lengthened and more screens were added to the settling chamber. This was done to further reduce the freestream turbulence. These modifications

are not expected to have any effect on the measurement of the low wavenumber components of the turbulent boundary layer.

The test configuration for the zero gradient work is shown in Figure (3.2). Because the test section is enclosed in an airtight blockhouse, a free jet configuration can be used. One of the major sources of noise was believed to be sound generated by unsteady flow in the diffuser, so the ducting between the test section and the diffuser was removed to allow some of the sound to propagate into the blockhouse. A foam-covered collector was placed on the entrance to the diffuser. The blockhouse was made as absorptive as possible by covering the walls, floor, and ceiling with two inches of polyurethane foam. To further quiet the tunnel, damping material was placed on the blower housing and on the bellmouth of the blower.

One of the problems encountered early in the test program was the excitation of the first order longitudinal room mode of the blockhouse at a frequency of 40 Hz. At some free-stream velocities, the sound pressure level in the blockhouse in a third octave band around 40 Hz would be as high as 117 dB relative to 20 μPa (.0002 μbar). One possible source of excitation was eddies being shed from the rear of the test section and impinging on the diffuser. This was reduced by adding triangular splitter plates to the rear of the test section. To add damping to the room at low frequencies, lead-vinyl sheeting was hung in the blockhouse. This treatmeant

reduced the aforesaid sound pressure level in the blockhouse in the third octave band around 40 Hz to 85 dB.

The ducting was 15 inches by 15 inches in cross section. Inside the blockhouse there were two sections of ducting, a six-foot section of sand-loaded ducting and then a three-foot test section. For the zero gradient tests, the boundary layer was allowed to develop naturally on the bottom wall of the ducting. The plates were flush-mounted in the center of the test section. The test speeds were 20, 25, 30, and 35 meters per second.

The boundary layer profiles were measured at the center of the plate using a United Sensor .040" total head tube and a static tap in the test section floor. The pressure differences were read on a Betz micromanometer. The boundary layer parameters displacement thickness, δ^*; and momentum thickness, θ, were calculated by integrating the boundary layer profiles and the shape factor, $H = \delta^*/\theta$, was then determined. By fitting the boundary layer profile data to a law of the wall, the friction velocity, U_τ, was determined from the slope of the logarithmic overlap region of the law of the wall. Single-point wall pressure spectra were also measured. The results of the single point wall pressure spectrum measurements are shown in Figure (3.3) along with Burton's [2] and Blake's [1] measurements. All of the data taken were reasonable for a turbulent boundary layer on a flat plate with a zero pressure gradient and are summarized in Table (3.1).

The configuration for the adverse gradient work was made similar to the one used by Burton [2] and is shown in Figure (3.4). Burton [2] made cross-spectral density measurements in an adverse gradient in the same facility. In order to permit utilization of Burton's cross-spectral density data, the adverse gradient and test section parameters were made to correspond closely with those of Burton [2].

The setup in the blockhouse was similar to that used for the zero gradient measurements in that there was upstream ducting, a test section, and then the air was allowed to jet freely to a foam-covered collector. The adverse gradient was created by spline-fitting a damped piece of aluminum between the bottom wall of the upstream ducting and the bottom wall of the test section. The bottom wall of the test section was set at an angle of 14^{o} to the horizontal. The proper angle was determined experimentally by applying the criterion that the desired gradient was the most severe gradient that would not cause separation on the tested surface. The flow speed for the tests was 30 meters per second.

The plates were flush-mounted in the bottom of the test section. The test section of Burton [2], as well as the one used in the adverse gradient tests, was 12 inches long. The wavenumber filters are 7 inches long and were mounted in

two separate positions in the test section, as shown in Figure (3.5).

Boundary layer profiles were measured every two inches along the test section. The displacement thickness, momentum thickness, and shape factor were calculated from the boundary layer profiles and are listed in Table (3.2). They are plotted in Figure (3.6) along with Burton's [2] as a function of downstream distance. The nondimensional pressure gradient $(\delta^*/Q)(dp/dx)$ is plotted against downstream distance in Figure (3.7). The outer boundary layer parameters for the adverse gradient tests were similar to those obtained by Burton [2] in the same facility, as can be seen from Figure (3.6).

3.2 The Wavenumber Filters

The two new wavenumber filters were designed and constructed by using guidelines given by Martin [11] and clamped plate eigenvalues from Leissa [13]. One of the new wavenumber filters was made of brass and the other from steel; both were designed for studying the same nondimensional frequency range. The two filters have the same surface dimensions, L_1 and L_3 and so the modal wavenumbers are identical for the same mode numbers. The corresponding resonant frequencies are slightly different. Hence on a k_1, ω plot the two filters increase the data along lines of constant k_1, as can be seen in Figure (2.3).

The modal damping factors were determined experimentally for each mode of both plates. The fact that the modal damping factors are different adds desirable redundancy to the data because it is difficult to get repeatable damping measurements. The nondimensional frequency range of interest was $5.0 < \omega\delta^*/U_\infty < 10.0$ which was estimated to correspond to a modal resonance frequency range of 2 kHz to 9 kHz.

The physical characteristics of the wavenumber filters are:

A. Brass Filter

a. Surface Dimensions: $L_1 = 0.178$ meters
$L_3 = 0.027$ meters

b. Thickness: 3.81×10^{-4} meters

c. Surface Density: 3.32 kg/m^2

B. Steel Filter

a. Surface Dimensions: $L_1 = 0.178$ meters
$L_3 = 0.027$ meters

b. Thickness: 2.54×10^{-4} meters

c. Surface Density: 2.06 kg/m^2

The plates were rigidly epoxied to heavy steel frames. The frame mass was much greater than the plate mass to reduce the vibration transmitted from the plate to the frame.

In designing the new wavenumber filters, it was desired to have low levels of acoustic contamination, low

levels of convective ridge contamination, and no modal overlap in the frequency range of interest. In order to reduce the acoustic contamination, the plates' modal wavenumbers were made almost twice the acoustic wavenumber. The plates were rigidly epoxied to the steel frames, thus approximating clamped boundary conditions. One of the results of Martin [11] is that clamped boundary conditions are superior to simple supports for reduction of convective response of the plate. The use of a plate elongated in the flow direction also reduces convective ridge contamination. In addition, the use of an elongated plate reduces the chance of modal overlap in the frequency range of interest because the frequencies of the $n=2$ modes are much higher than the frequencies of the $n=1$ modes of interest.

3.3 Determination of Modal Characteristics

The modal characteristics needed to relate the wavenumber frequency spectrum to the plate acceleration response are the modal mass, the modal frequencies, and the modal damping factors. These quantities were determined experimentally.

The plate's surface density was determined by measuring accurately the dimensions of the plate and then measuring carefully the plate's mass.

The modes of the plate were identified by exciting the plate over a small area with an acoustic driver and observing

the Chladni patterns that were formed. The odd/odd modes of the plates with unity lateral index from the 3,1 mode to the 5,1 mode were identified. The modal frequencies were determined at the same time.

The modal damping factors, η_{mn}, were determined experimentally by measuring decay rates. The experimental setup is shown in Figure (3.7). The plates were excited with an acoustic driver at resonance; the driver was shut off and the decaying transient was recorded. The plate acceleration was monitored at the center of the plate with a 0.2 gram Wilcoxon model 91 accelerometer. All of the damping measurements were made with the plates mounted in the bottom of the test section. The decay of the sound field was measured to insure that the measured decay rate was due to structural and radiation damping and not due to the decaying sound field. When the acoustic driver was turned off, the decaying acceleration transient was recorded on a B & K model 7502 digital event recorder. The signal was played back at a lower speed into a B & K model 2305 graphic level recorder. The graphic level recorder gave a record of the rms level of the transient signal. The transient signal decayed very rapidly so it was necessary to record it and then play it back at a lower speed to get repeatable results. This procedure was considered more accurate than measuring the 3 dB down points

from resonant response. The damping factors were determined from the decay records for each mode of interest (Figure 3.8). The equivalent rectangular bandwidths of each mode were then determined from

$$\Delta f_{mn} = \frac{\pi}{2} \eta_{mn} f_{mn} \qquad (3.4)$$

Table (3.3) is a compilation of modal frequencies, damping factors, and equivalent rectangular bandwidths.

3.4 Measurement of Plate Response

The acceleration response of each plate was measured at the center of the plate. The equipment setup was the same for both the zero-gradient and adverse gradient experiments.

The plate's acceleration was measured with a Wilcoxon model 91 accelerometer. The signal from the accelerometer went into an Ithaco model 432 low noise preamplifier and then into an Ithaco model 4213 band pass filter. A Federal Scientific model UA15A spectrum analyzer was used to measure the acceleration spectra. A Federal Scientific model 1015 spectrum averager was used to average the sample spectra 512 times. This was done to increase the statistical accuracy of the data. The spectra were then recorded on a Varian model F-50 x-y plotter.

The noise bandwidth of the spectrum analyzer was 32 Hz for the 10 kHz analysis range. It is customary to report data

in terms of spectrum level, i.e., the one Hertz band level. For broadband signals this is done by dividing the analyzer output by the bandwidth of the analyzer. However, the equivalent modal bandwidths are sometimes smaller than the noise bandwidth of the analyzer. For example, consider the (9,1) mode of the brass plate with an equivalent modal bandwidth of 12.6 Hz and the 10 kHz analysis range with a bandwidth of 32 Hz. It would be inappropriate to calculate the measured acceleration spectral level based on the 32 Hz analyzer bandwidth because most of the measured mean square acceleration response is in the 12.6 Hz equivalent modal bandwidth. In order to correctly determine the spectral density at the resonant peaks, it is necessary to compare the plate's modal bandwidth with the analyzer bandwidth and use the smaller one. On the 10 kHz analysis range, the plate's modal bandwidths were generally smaller, but on the 5 kHz analysis range the analyzer bandwidth tended to be smaller. When the appropriate bandwidths were used to obtain spectral density levels, there was good agreement between the data taken on the 10 kHz analysis ragne and the data taken on the 5 kHz analysis range.

Two sample plate acceleration spectra are shown in Figures (3.9) and (3.10). Figure (3.9) is a sample spectrum for the brass plate and Figure (3.10) is a sample spectrum for the steel plate. For illustrative purposes the spectra were

determined from the analyzer bandwidth in the figures. Only the resonant peaks are useful in determining low wavenumber levels. From Figures (3.9) and (3.10), the resonant peaks can easily be identified. The odd-odd modes are well separated in frequency and are considerably above the noise floor.

4. EVALUATION OF ZERO GRADIENT RESULTS

The plate in the wind tunnel responds to three separate sources of excitation: acoustic, convective and low wavenumber. In order to be sure that the low wavenumber components are actually measured, careful evaluation of possible contamination by the other two sources is important. In section 4.1 and 4.2 the plate acceleration response is compared with acoustic and convective contaminating levels.

If the data are not contaminated the results of the last two chapters can be used to obtain the low wavenumber levels from the plate acceleration spectral levels. These low wavenumber levels can then be compared with the results of other investigations. Farabee and Geib [7] have microphone array data in the same nondimensional frequency range. There is also a small region of overlap with Martin's [11] data.

4.1 Comparison with Estimated Acoustic Response

An analytic method for making estimates of the plate response to acoustic excitation was presented in Section 2.5. The result is expressed in Equation (2.16) and depends on the acoustic level in the blockhouse, $\Phi_A(\omega_{mn})$. The acoustic level in the blockhouse was determined experimentally. The experimental acoustic levels, $\Phi_A(f)$, are related to the theoretical acoustic levels, $\Phi_A(\omega)$ by

$$\Phi_A(f) = 4\pi\Phi_A(\omega). \qquad (4.1)$$

The acoustic levels in the blockhouse were measured at three locations inside the blockhouse using a one inch Bruel & Kjaer microphone. A microphone could not be placed directly in the flow because its response would be dominated by self noise and not be an accurate representation of the acoustic levels in the blockhouse. There was a small variation in levels between microphone positions. The data used to estimate the acoustic levels at the plate were taken halfway between the test section and the collector. Figure (4.1) is a sample spectrum of the background noise. It is believed that one of the major sources of noise in the wind tunnel is unsteady flow in the diffuser. If this is actually the case then the acoustic levels at the plate should be lower than the acoustic levels measured farther downstream. In order to be conservative, i.e. to give a high estimate, the measured acoustic levels were used to estimate the plate response. The measured acceleration levels are plotted with the estimated acoustic response in Figures (4.2) and (4.3) for the brass plate at 20 m/sec and 35 m/sec, respectively. In these plots only the points shown are valid data points, the lines were drawn between the points to indicate trends in the data.

Only two data points were within 5 dB of the estimated acoustic response. Both points were corrected for their nearness to the estimated acoustic levels. There were no points

eliminated because of acoustic contamination for the zero gradient data.

4.2 Comparison with Estimated Convective Response

The convective response of the plates were evaluated by using the model developed for this purpose by Martin [11] and the experimentally determined plate parameters. The response was calculated from Equation (2.15), which depends on the single point wall pressure spectrum of the turbulent boundary layer. Both Blake [1] and Burton [2] measured the single point spectrum in this facility. In the nondimensional frequency range of interest Blake's [1] data are slightly higher and agree with current measurements of the single point wall pressure spectrum and so are used to evaluate Equation (2.15). The value of convection velocity, U_c, used to evaluate the convective response was $0.6U_\infty$. If this value, $0.6U_\infty$, is substituted into Equation (2.15) it can be shown that the convective ridge levels are proportional to U_∞^{11} for a fully clamped plate, assuming that the single point wall pressure spectrum is proportional to U_∞^4.

Convective contamination becomes increasingly significant with increasing free stream velocity. The estimated convective contaminating levels are plotted along with the

measured plate acceleration levels for the brass plate in Figures (4.2) and (4.3) for 20m/sec and 35m/sec, respectively. For the flow velocities used in this study the convective levels were well below the measured plate acceleration levels.

4.3 Measured Low Wavenumber Levels, $P(k_1^*,o,\omega^*)$

In order to make comparisons with other investigators' data, the measured low wavenumber levels, $P(k_1,o,\omega)$ were nondimensionalized on outer boundary layer parameters. The nondimensionalization used was $q^2\delta^{*3}/U_\infty$, where q is the dynamic pressure ($\frac{1}{2}\rho U_\infty^2$), δ^* is the boundary layer displacement thickness, and U_∞ is the free stream velocity. The wavenumber and frequency are also nondimensionalized as in Equation (2.6). The result is

$$P^*(k_1^*,o,\omega^*) = P(k_1^*,o,\omega^*)/(q^2\delta^{*3}/U_\infty). \qquad (4.2)$$

The measured low wavenumber levels are presented in Tables (4.1) and (4.2) for the brass and steel plates, respectively.

In interpreting the data it is important to recognize what is actually measured. Each spectrum level in Tables (4.1) and (4.2) should be interpreted as a level of $P(k_1^*,o,\omega^*)$ averaged over the wavenumber-frequency domain of the corresponding resonant mode. The frequency domain of each measured

level is defined by the resonance frequency of the mode and its corresponding equivalent rectangular bandwidth. The wavenumber domain is characterized by both a k_1 and k_3 bandwidth. The k_1 bandwidth Δk_1 is $2\pi/L_1$, which for this study is 35.5 $(\text{meters})^{-1}$ and the k_3 bandwidth Δk_3 is approximately $9.09/L_3$ which for this study is 340.8 $(\text{meters})^{-1}$. Since only the first order lateral modes were considered, each wavenumber region is centered on $k_3 = 0$ and $k_1 = k_m \simeq (m + \frac{1}{2})\pi/L_1$. The value of k_m and ω_{mn} locate the measured low wavenumber levels in wavenumber-frequency space.

In an effort to ascertain the dependence of the low wavenumber levels on k_1^* and ω^*, Figure (4.4) was prepared as a plot of contours of $P^*(K_1^*,o,\omega^*)$ = const. in k_1^*,ω^* space. The numbers beside the points indicate the level of $P^*(k_1^*,o,\omega^*)$ in Figure (4.4). There is a great deal of scatter in the data and only general trends can be observed from Figure (4.4). The low wavenumber levels are decreasing with increasing ω^*. The trend in k_1^* is not as clear. Careful inspection of Figure (4.4) tends to show the low wavenumber levels decreasing with increasing k_1^*. This result is physically unrealistic because increasing k_1^* moves one closer to the convective ridge and so the expected dependence is the opposite of the observed.

Martin [11] observed only a very small positive k_1^* dependence. Therefore the real dependence on k_1^* may be obscured by the overall scatter of the data.

It was possible to quantify the ω^* dependence of the two plates assuming a negligible k_1^* dependence. The least squares model used was

$$10 \text{ Log } \{P^*(k_1^*,o,\omega^*)\} = C_1[10 \text{ Log } \omega^*] + C_2 \qquad (4.3)$$

Standard least square techniques were used, and the coefficients were evaluated as $C_1 = -3.87$ and $C_2 = -80.9$. The resulting nondimensional frequency dependence is $(\omega^*)^{-3.87}$. The data points, $P^*(k_1^*,o,\omega^*)$ and the least squares fit to the data are shown in Figure (4.5). The brass and steel plates are in excellent agreement, as can be seen in Figure (4.5).

4.4 Comparison with Other Investigators

The results of other investigators are shown in Figure (4.6) along with the current results. Figure (4.6) shows only ω^* dependence under the assumption that the spectrum is independent of k_1^* for small values of k_1^*. The data of Farabee and Geib [7] in the region $5 < \omega\delta^*/U_\infty < 10$ are directly comparable with the current data. The wavenumber range of the current data is $0.56 < k_1\,\delta^* < 1.80$ and $k_3\,\delta^* = 0$ and the

wavenumber range of the data of Farabee and Geib is $1.34 < k_1\delta^* < 1.38$ and $k_3\omega^* = 0$. The data of Farabee and Geib [7] were taken using an array of microphones as a spatial filter. In the region of direct comparison, the data of Farabee and Geib were from 1 to 5 dB above the average of the current data but within the scatter of the current data. In the range $5 < \omega\delta^*/U_\infty < 10$, Farabee and Geib report an ω^* dependence of $(\omega^*)^{-5}$ compared with the ω^* dependence of $(\omega^*)^{-3.87}$ observed in the current results. In the region $10 < \omega\delta^*/U_\infty < 30$, $k_1\delta^* = 1.72$, $k_3\omega^* = 0$, Farabee and Geib report an ω^* dependence of $(\omega^*)^{-4}$ which agrees well with current results. There are a few data points in the region $10 < \omega\delta^*/U_\infty < 30$ to compare with the data of Farabee and Geib. These points lie about 7 dB above the microphone data of Farabee and Geib.

There is also a small region of direct overlap in wavenumber-frequency space with Martin [11]. Some points from Martin as well as the least squares fit to Martin's data are shown in Figure (4.6). In the region of direct comparison the current data lie about 5 dB above Martin's data. Jameson [10] also reported low wavenumber data in the same nondimensional frequency range as Martin but a different wavenumber range.

Both Jameson [10] and Martin [11] used the spatial filtering of plates to obtain their data. Martin's plates were

.508m by .0762m with the long dimension oriented with the flow. Martin used the (3,1) mode to the (21,1) mode, which corresponds to a wavenumber range of $0.2 < k_1 \delta^* < 1.0$ and $k_3 \delta^* = 0$. Jamesons' plates were .27m by .18m with the long dimensions oriented with the flow. Jameson identified several distinct modes that correspond to a wavenumber range of $.12 < k_1 \delta^* < .28$ and $0 < k_3 \delta^* < .24$. The levels reported by Jameson tended to be 10 dB lower than the levels reported by Martin. This discrepancy has not been adequately explained. The ω^* dependence of Martin; $(\omega^*)^{-3.65}$ is very similar to the $(\omega^*)^{-3.87}$ dependence of the current results and seem to agree with the ω^* dependence of Jameson.

The current data behave similarly to the data of Martin and Jameson in that there is a large amount of scatter in the data. This imperfect collapse on outer boundary layer parameters in typical of measurements using a plate as a spatial filter.

5. ADVERSE GRADIENT RESULTS

As reported in Sections 5.2 and 5.3 below, the adverse gradient data were checked for contamination by both acoustic levels in the blockhouse and convective ridge levels. Where the data were not contaminated, they could then be analyzed for the effect of flow inhomogeneity on the low wavenumber levels. This is discussed in Sections 5.1 and 5.4.

5.1 Anticipated Effects of the Adverse Gradient

The adverse gradient experiments were conducted to study the effect of flow inhomogeneity upon the response of structures at low wavenumbers. A severe inhomogeneity in the direction of flow was caused by a strong adverse gradient which forced the boundary layer to thicken rapidly towards separation. When the flow lacks homogeneity the wall pressure spectrum is a function of two vector wavenumbers, viz., $\Phi_p(\bar{k},\bar{K},\omega)$. The wall pressure spectrum still has a maximum along a convective ridge where $k_1 = \omega/U_c$ and $k_3 = 0$. However, another maximum should occur for $\bar{k}$ very small where the $\bar{k}$ dependence is characterized by the scale of the inhomogeneity. The expected result was that the streamwise inhomogeneity would contribute to the low wavenumber levels of the turbulent boundary layer. This did not occur and the levels tend to

agree with the zero gradient levels based on the analysis of Section 5.4.

5.2 Comparison With Estimated Acoustic Response

In order to evaluate the acoustic response of the plate it is necessary to know accurately the acoustic level in the blockhouse. The acoustic levels in the blockhouse were determined experimentally with a Bruel and Kjaer one inch microphone placed halfway between the test section and the collector.

In the final tested configuration shown in Figure (3.4), there were some problems in determining the acoustic levels in the blockhouse. The signal from the microphone had a very large transient component that limited the amplification of the signal and caused analyzer noise floor problems.

The cause of the transient was believed to be buffeting of the microphone. This was caused by the divergence of the flow due to the adverse gradient configuration. The collector did not lie in line with the mean flow, and there was some flow reversal under the collector. As a result, the microphone might have been limited by its own self noise. In Figure (5.1) the measured noise levels are shown along with earlier noise levels measured with a divergence angle in the test section 12^{o}. This earlier measurement did not have a problem with large transients. Also shown is a zero gradient

noise spectrum for the same flow speed. In Figure (5.1), it can be observed that the noise spectrum measured for the final configuration does not exhibit the same character as the other two spectra. Although the noise spectrum measured for the final configuration is believed to be high, it is used to evaluate the acoustic contamination so that the estimated acoustic levels are conservative, i.e. high estimates of acoustic contamination.

In Figure (5.2) and (5.3) the measured levels are plotted along with the estimated acoustic response based on the final configuration noise levels for the brass and steel plates. If the acoustic levels measured for the final configuration are indeed representative of the true acoustic levels in the blockhouse then much of the adverse gradient data are acoustically limited. If the levels measured for the 12 degree divergence angle are more typical of the true acoustic levels in the blockhouse, then most of the data are useful. In either case further analysis is justified if only to establish a noise floor for the low wavenumber response in an adverse gradient.

5.3 Comparison to Estimated Convective Response

The convective response of the plates can be estimated by using the data for cross spectral density of an adverse gradient boundary layer and convection velocities provided by Burton [2] and a model to estimate convective response.

At thirty meters per second for the test configuration for zero gradient, the convective ridge levels are considerably lower than the measured levels. For the adverse gradient configuration of the same upstream tunnel velocity the convection velocity is decreasing, thus increasing the separation in wavenumber of the convective ridge and the model wavenumbers of the plates. The adverse gradient does cause some spreading of the convective ridge in k_1^* and this effect could be important.

A crude model for this purpose was developed by using experimental fits to Burton's [2] data. The model is

$$\text{a.} \quad \Phi_p(k_1, k_3\omega) = 2.25\, \Phi_p(\omega) \left[\frac{U_\infty}{\omega}\right]^2$$

$$\text{for} \quad \left|k_1 - \frac{\omega}{U_c}\right| < .15\, \pi\, \frac{\omega}{U_c}$$

$$\text{and} \quad \left|k_3\right| < .3\pi\, \frac{\omega}{U_c}$$

$$\text{b.} \quad \Phi_p(k_1, k_3, \omega) = 0, \text{ elsewhere.} \qquad (5.1)$$

This model is used to evaluate equation (2.5) along with an asysmptotic form for the wavenumber filter shape. The estimated acceleration spectral response of the plates to convective excitation can be expressed by

$$S_a\left(\frac{L_1}{2},\frac{L_3}{2},\ \omega_{mn}\right) = \frac{85.75\ k_m^4}{L_1^2 L_3\ (\sigma\eta)^2_{mn}}\ \Phi_p(\omega_{mn})\left(\frac{\omega_{mn}}{U_\infty}\right)^{-7} \qquad (5.2)$$

This predicts levels 12 dB higher than the similar expression for the zero gradient case. This rough analysis predicts that the convective ridge levels are still well below the measured acceleration levels.

5.4 Analysis of the Adverse Gradient Response

In our analysis of the adverse gradient response, the flow inhomogeneity was neglected and the data were reduced using center-of-tne-plate values for the boundary layer parameters, and the results of Chapter 2.

The low wavenumber levels measured for the adverse gradient case were nondimensionalized on outer boundary layer parameters with center-of-the-plate values. The results are listed in Tables (5.1) and (5.2) and are shown graphically in Figure (5.4). The data exhibit the scatter typical of other low wavenumber measurements using the spatial filtering

characteristics of fully clamped plates. In Figure (5.4) the circled points are those that are acoustically limited when the acoustic levels measured for the final test configuration are used. The levels that are apparently contaminated agree with and tend to lie below the uncontaminated data. This suggests that there was undetermined circuit or flow noise in the measured acoustic levels used to evaluate the acoustic contamination and perhaps the acoustic levels for the 12^{o} divergence angle of the test section are more representative.

In Figure (5.5) the adverse gradient results are shown along with the zero gradient results. The adverse gradient results seem to agree quite well with the zero gradient results.

Even if only an upper bound was determined for the adverse gradient case; it is evident that the severe inhomogeneity in the mean flow did not considerably increase the low wavenumber levels. A more detailed analysis was not performed because the expected increase in low wavenumber levels due to the adverse gradient did not occur.

6. CONCLUSIONS

6.1 Conclusions Regarding Zero Gradient Measurements

1) Low wavenumber measurements were made in the non-dimensional frequency and wavenumber region: $0.56 < k_1 \delta^* < 1.80$, $k_3\delta^* = 0$, and $3 < \omega\delta^*/U_\infty < 10$. The data exhibit an $(\omega\delta^*/U_\infty)^{-3.87}$ frequency dependence but no significant $k_1\delta^*$ dependence.

2) The measured plate accleration levels were too high to be accounted for by either acoustic or convective ridge excitation, therefore the data would appear to be a representation of the low wavenumber components of the turbulent boundary layer.

3) Farabee and Geib [7] have taken microphone array data in the same nondimensional frequency and wave-number region as the current data. The current data compare well with the levels measured by Farabee and Geib but show a different frequency dependence. In the region of nondimensional frequency and wavenumber overlap with Martin's [11] data, the current data are slightly higher but show the same frequency dependence.

6.2 Conclusions Regarding Adverse Gradient Measurements

1) There is an indication that the levels measured for the advance gradient case might be acoustically

limited. The convective ridge levels are well below the measured levels.

2) The imposition of a severe inhomogeneity on the mean flow did not significantly increase the low-wavenumber levels.

U_∞ (m/sec)	R_{e_θ}	δ (inch)	θ (inch)	$H = \delta^*/\theta$	U_T/U_∞
20	6.3×10^3	.242	.187	1.30	.031
25	8.0×10^3	.250	.188	1.33	.033
30	9.4×10^3	.227	.185	1.23	.036
35	11.5×10^3	.265	.194	1.37	.033

Table 3.1 Mean Properties of the Zero Gradient Boundary Layers

Station	U_∞/(m/sec)	Re_θ	δ^*/(inch)	θ/(inch)	$H=\delta^*/\theta$
0	31.5	10.3×10^3	.284	.193	1.47
2	30.4	11.5×10^3	.344	.223	1.54
4	29.8	12.6×10^3	.399	.250	1.59
6	29.2	14.9×10^3	.519	.302	1.72
8	28.4	16.4×10^3	.623	.340	1.83
10	28.0	18.4×10^3	.768	.389	1.98
12	27.5	20.3×10^3	.933	.436	2.14

Table 3.2 Mean Properties of the Adverse Gradient Boundary Layer

Plate	Mode	Frequency f_{mn}/Hz	Damping Factor η_{mn}	Equivalent Bandwidth Δf_{mn}/Hz
Brass	5.1	2322	.00555	20.2
	7.1	2716	.00266	11.4
	9.1	3300	.00243	12.6
	11.1	4072	.00474	30.3
	13.1	5024	.00245	19.3
	15.1	6130	.00237	22.8
Steel	5.1	2250	.00552	19.5
	7.1	2588	.00346	14.1
	9.1	3117	.00356	17.4
	11.1	3833	.00363	21.9
	13.1	4725	.00342	25.4
	15.1	5786	.00402	36.5

Table 3.3 Experimentally Determined Plate Characteristics

U_∞ (m/sec)	$\omega\delta^*/U_\infty$	$k_1\delta^*$	$P^*(k_1^*,o,\omega^*)$
	4.58	0.60	-102.5
	5.39	0.82	-107.2
20	6.55	1.03	-111.4
	8.06	1.25	-114.0
	9.94	1.47	-115.4
	12.17	1.68	-126.0
	3.79	0.62	- 99.6
	4.45	0.84	-103.5
25	5.41	1.07	-108.3
	6.66	1.29	-111.0
	8.22	1.52	-111.3
	10.05	1.74	-119.8
	2.87	0.56	- 95.4
	3.37	0.76	- 98.9
30	4.10	0.97	-104.0
	5.04	1.17	-107.2
	6.22	1.38	-107.3
	7.61	1.58	-114.7
	2.80	0.64	- 99.1
	3.30	0.87	-102.6
35	4.01	1.10	-107.7
	4.93	1.34	-110.9
	6.08	1.57	-111.0
	7.44	1.80	-118.4

Table 4.1 Measured Levels of $P(k_1^*,0,\omega^*)$, $P^*(k_1^*,o,\omega^*) = 10\ \mathrm{Log}_{10}\ \{P(k_1^*,0,\omega^*)\ U_\infty/q^2\delta^{*3}\}$, Obtained with a Brass Plate in Zero Gradient Boundary Layer.

U_∞ (m/sec)	$\omega\delta^* U_\infty$	$k_1\delta^*$	$P^*(k_1^*,o,\omega^*)$
	4.33	0.60	-102.8
	5.00	0.82	-110.0
20	6.02	1.03	-112.5
	7.39	1.25	-112.1
	9.10	1.47	-122.4
	11.10	1.68	-126.1
	3.58	0.62	-100.9
	4.13	0.84	-106.5
25	4.97	1.07	-109.0
	6.11	1.29	-109.4
	7.52	1.52	-117.2
	9.18	1.74	-118.7
	2.71	0.56	- 97.7
	3.13	0.76	-101.7
30	3.76	0.97	-107.1
	4.62	1.17	-106.2
	5.69	1.38	-113.4
	6.94	1.56	-115.0
	2.65	0.64	- 97.9
	3.06	0.87	-102.4
35	3.68	1.10	-105.6
	4.52	1.34	-105.7
	5.57	1.57	-112.5
	6.74	1.80	-114.3

Table 4.2 Measured Levels of $P(k_1^*,o,\omega^*)$, $P^*(k_1^*,o,\omega^*) = 10\ \mathrm{Log}_{10}\ \{P(k_1^*,o,\omega^*)\ U_\infty/q^2\ \delta^{*3}\}$, Obtained with a Steel Plate in Zero Gradient Boundary Layer.

Position	$\omega\delta^*/U_\infty$	$k_1\delta^*$	$P^*(k_1^*,o,\omega^*)$
	4.76	0.95	-101.8
Brass Plate	5.57	1.30	-111.4
Position # 1	6.77	1.64	-110.1
	8.35	1.99	-110.7
	10.30	2.33	-116.4
	12.57	2.66	-122.4
	8.36	1.63	-107.4
Brass Plate	10.09	2.22	-116.9
Position # 2	12.26	2.81	-118.6
	15.13	3.40	-118.1
	18.67	3.99	-125.6
	22.77	4.58	-126.6

Table 5.1 Measurement of $P(k_1,o,\omega)$ in an Adverse Gradient Using Center of the Plate Values, $P^*(k_1^*,o,\omega^*) = 10 \text{ Log } \left\{P(k_1^*,o,\omega^*) \quad U_\infty/q^2\delta^{*3}\right\}$

Position	$\omega\delta^*/U_\infty$	$k_1\delta^*$	$P^*(k_1^*,o,\omega^*)$
	4.61	0.95	-106.5
Steel Plate	5.31	1.30	-111.8
Position # 1	6.40	1.64	-107.8
	7.86	1.99	-112.7
	9.68	2.33	-119.4
	11.86	2.66	120.2
	8.36	1.63	-111.2
Steel Plate	9.62	2.22	-120.0
Position # 2	11.58	2.81	-114.9
	14.24	3.40	-121.4
	17.55	3.99	-123.0
	21.50	4.58	-123.4

Table 5.2 Measurements of $P(k_1^*,o,\omega^*)$ in an Adverse Graident Using Center of the Plate Valves, $P^*(k_1^*,o,\omega^*)=$ 10 Log $\left\{P(k_1^*,o,\omega^*)U_\infty/q^2\delta^{*3}\right\}$

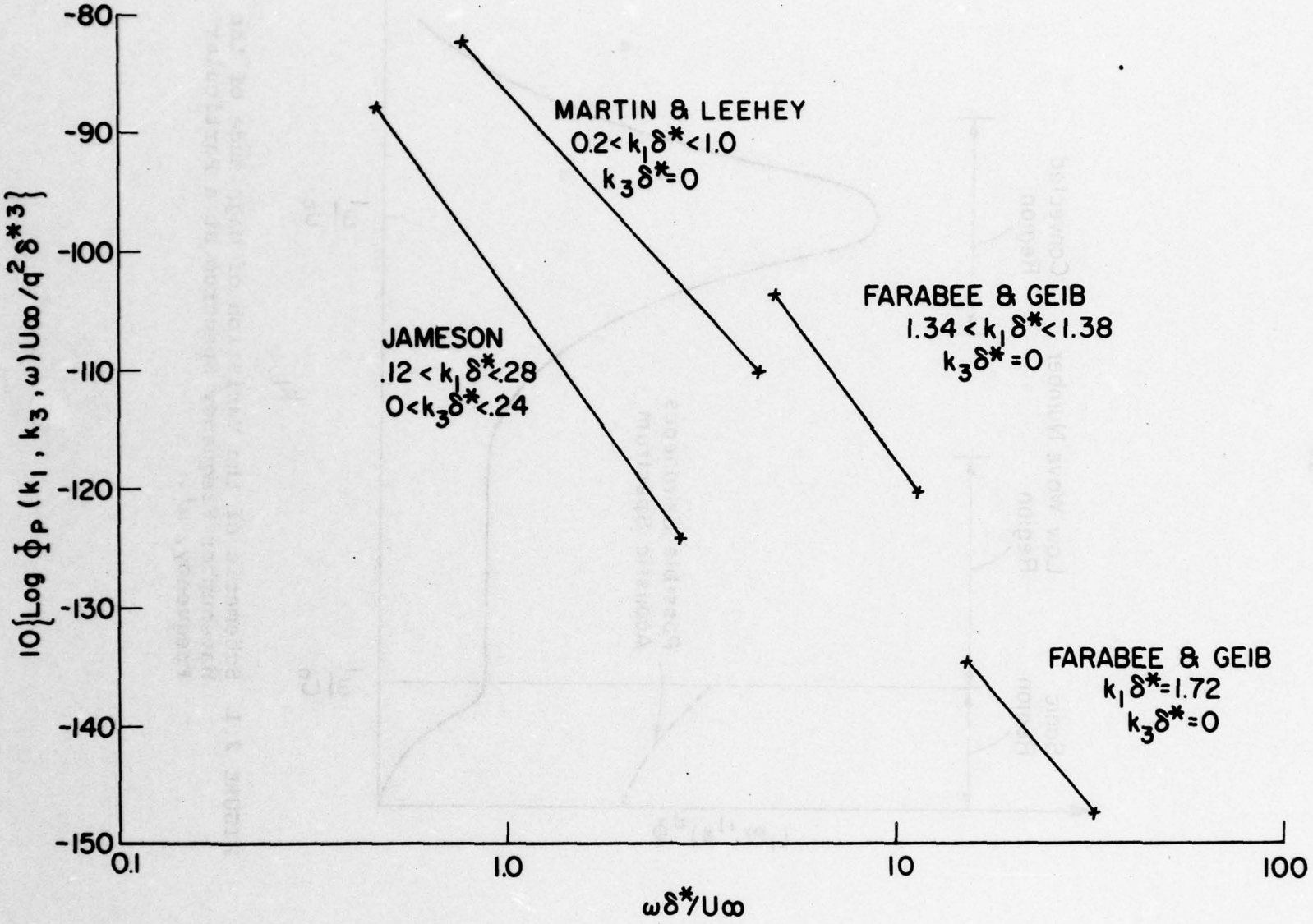

FIGURE 1.1 Low Wavenumber Data Reported by Other Investigators

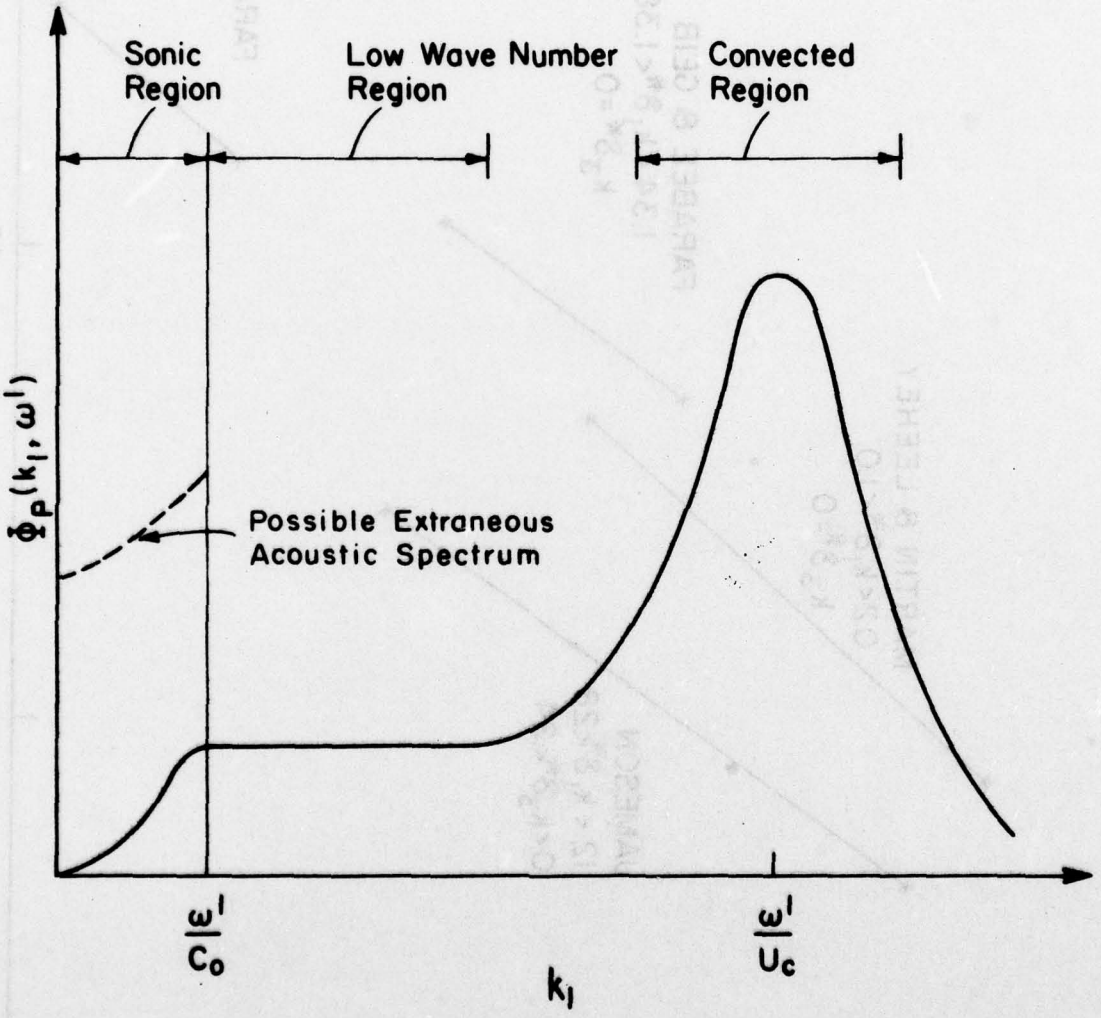

FIGURE 2.1 Schematic of the Variation of Magnitude of the Wavenumber Frequency Spectrum at a Particular Frequency, ω'.

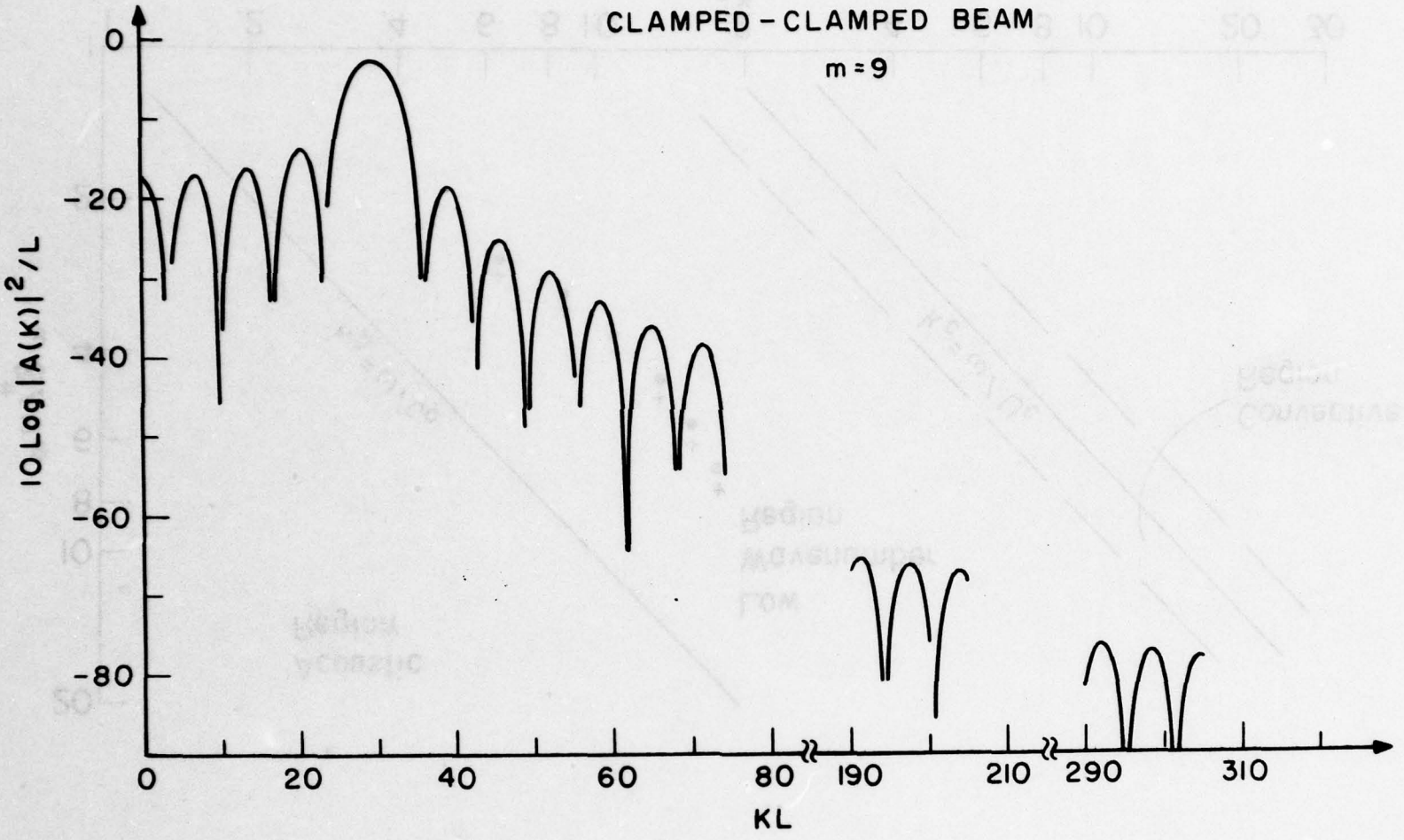

FIGURE 2.2 Wavenumber Filter Shape for a Clamped-Clamped Beam, m = 9.

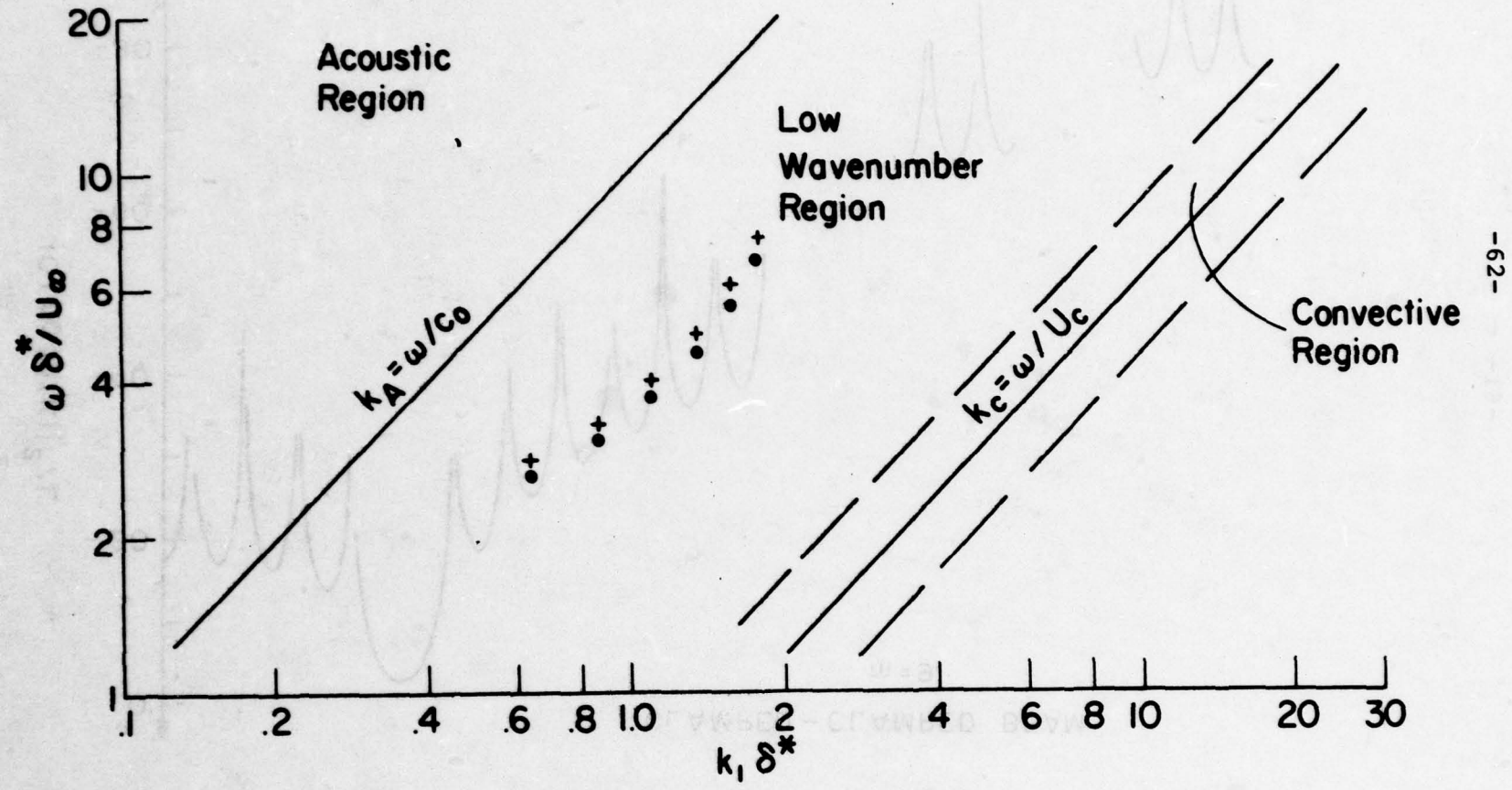

FIGURE 2.3 Wavenumber-Frequency Location of Various Excitations, U_∞ = 35 m/sec, C_o = 343 m/sec, + Brass Plate Modes, • Steel Plate Modes

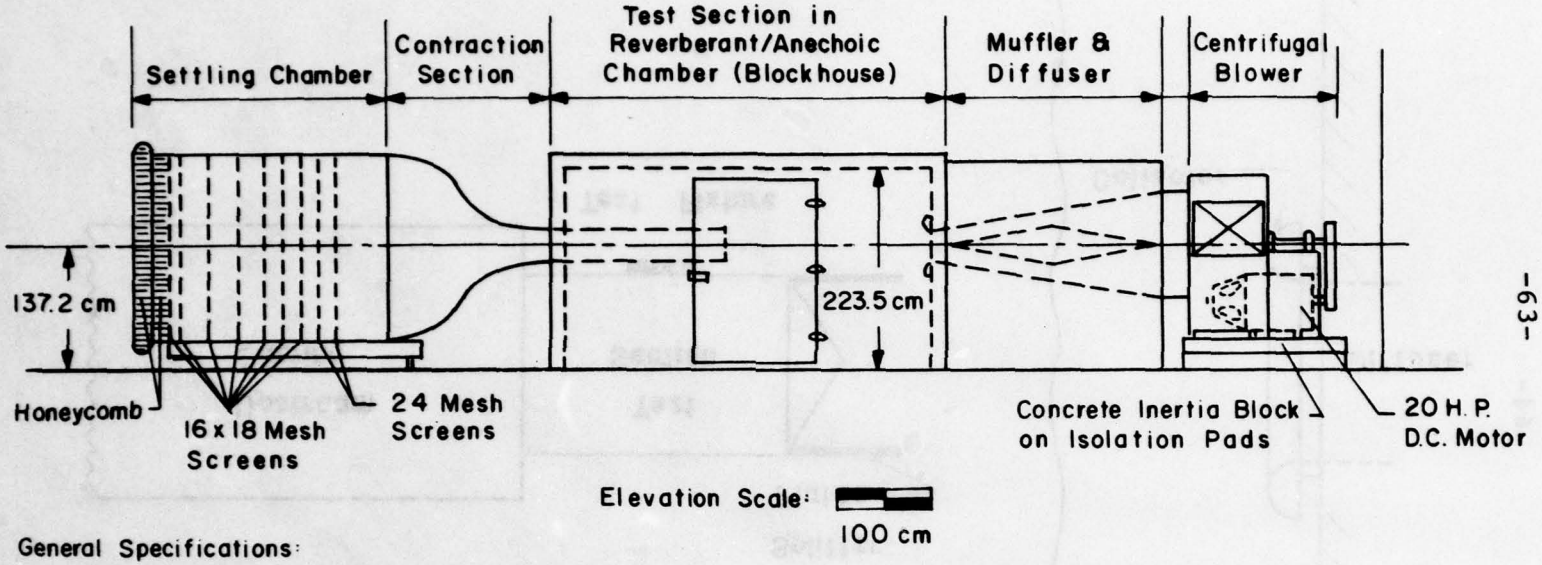

General Specifications:
Contraction Ratio: 20:1
Test Section: 38cm x 38cm, shown in open duct configuration

WIND TUNNEL FACILITY — ROOM 5-024
ACOUSTICS & VIBRATIONS LABORATORY
MASSACHUSETTS INSTITUTE OF TECHNOLOGY

FIGURE 3.1

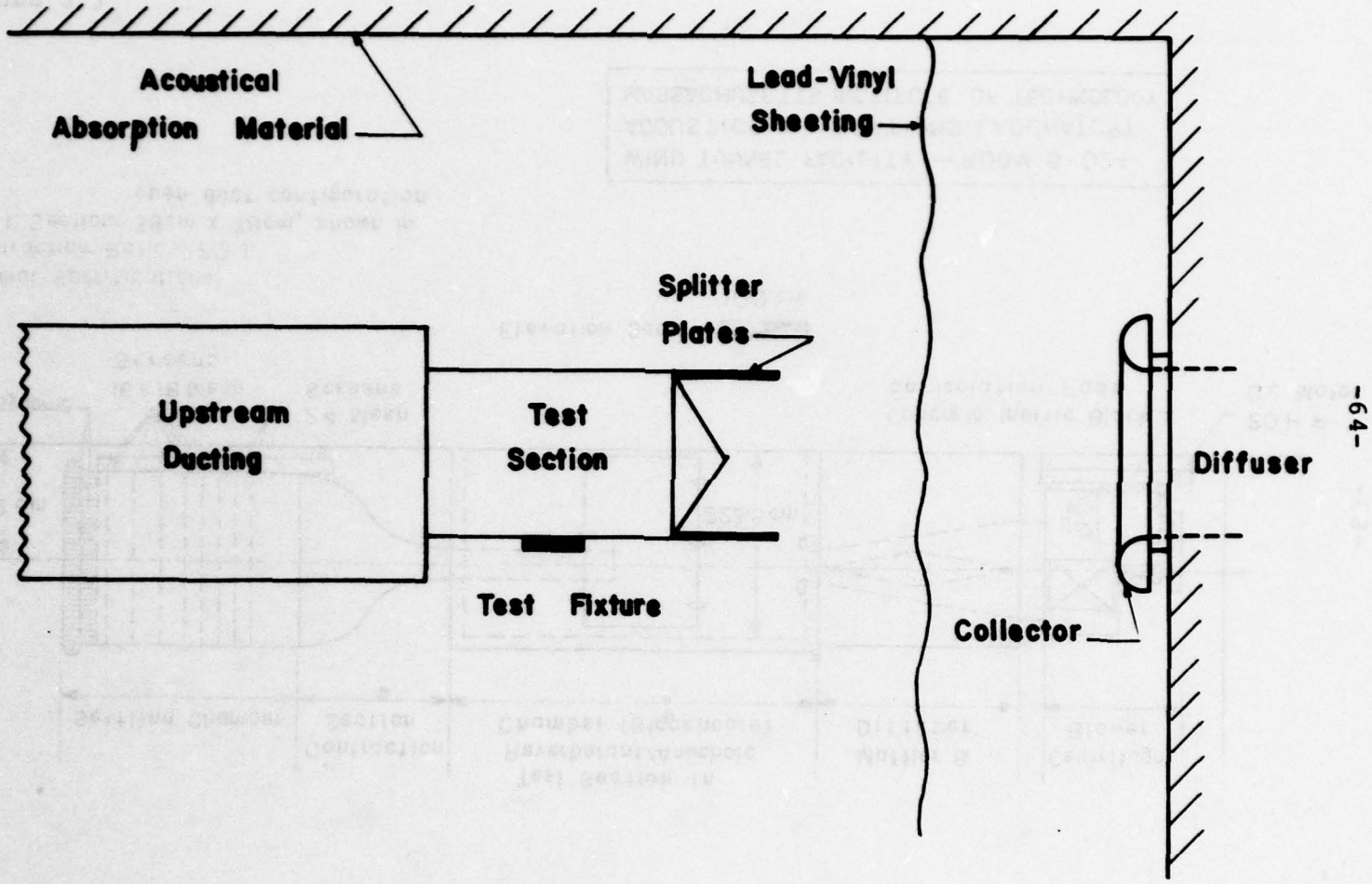

FIGURE 3.2 Test Configuration for Zero Gradient Experiments

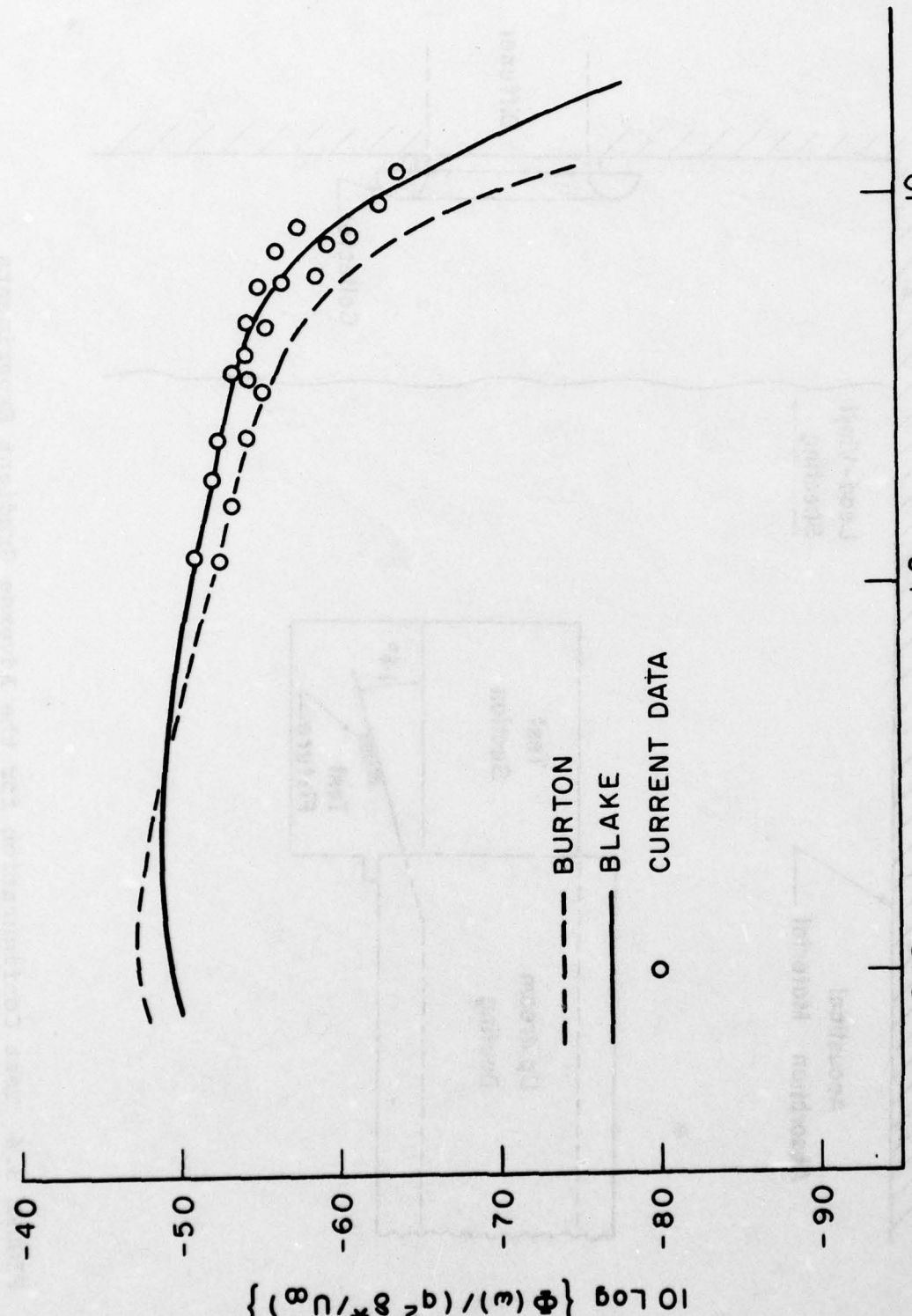

FIGURE 3.3 Wall Pressure Spectra, Data Not Corrected for Transducer Size Effects

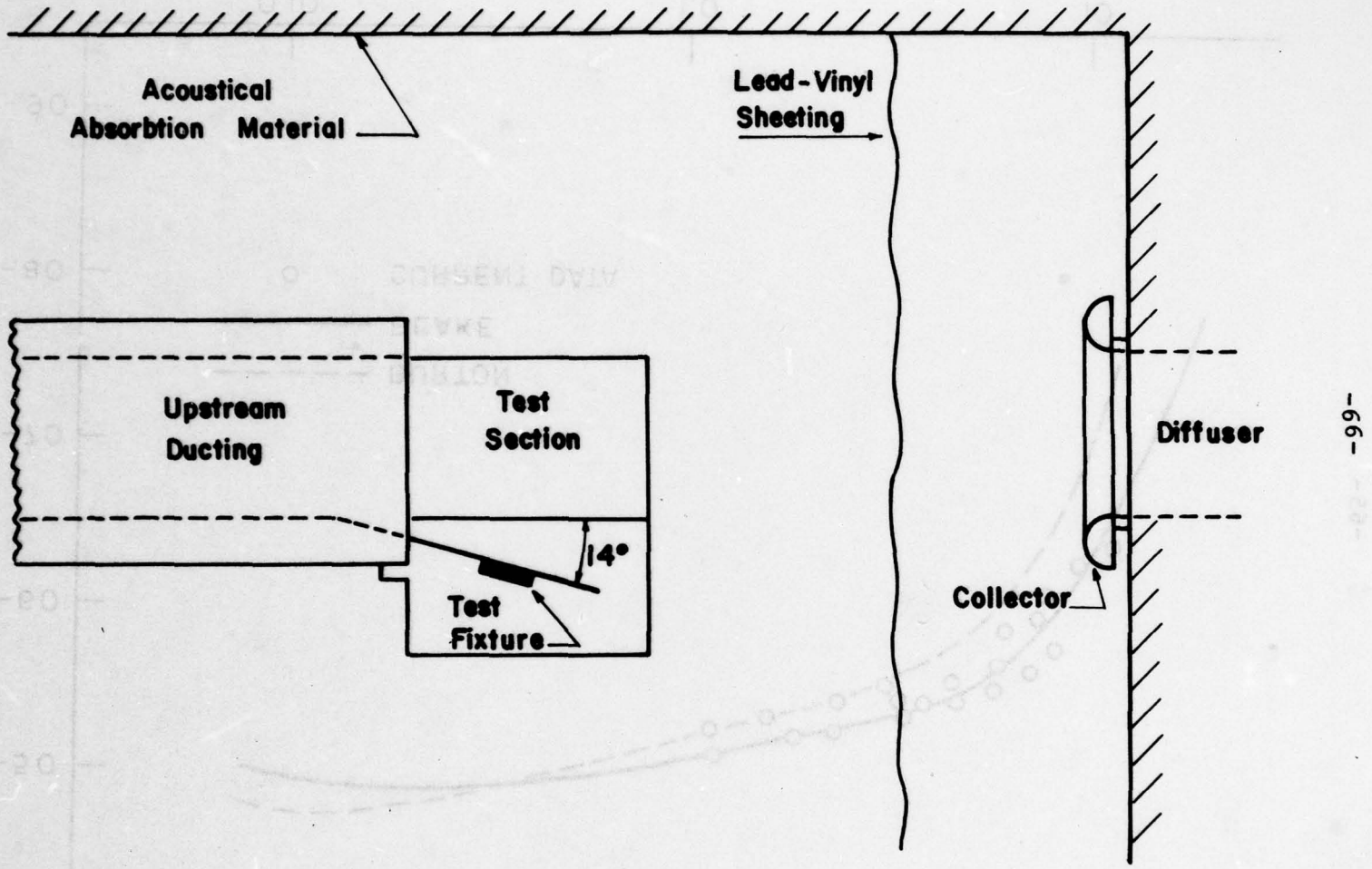

FIGURE 3.4 Test Configuration for the Adverse Gradient Experiments

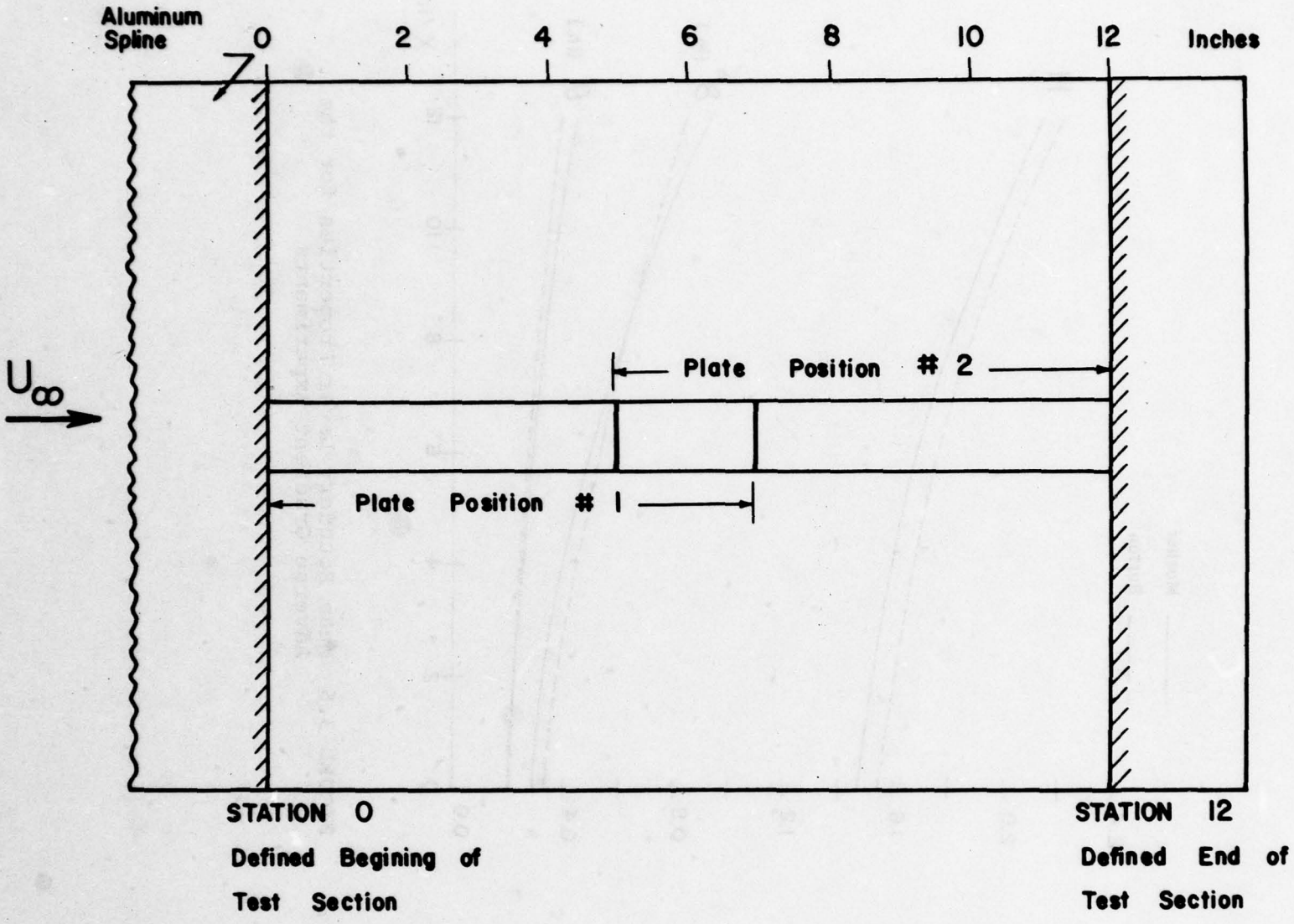

FIGURE 3.5 Defined Test Section for the Adverse Gradient Experiments

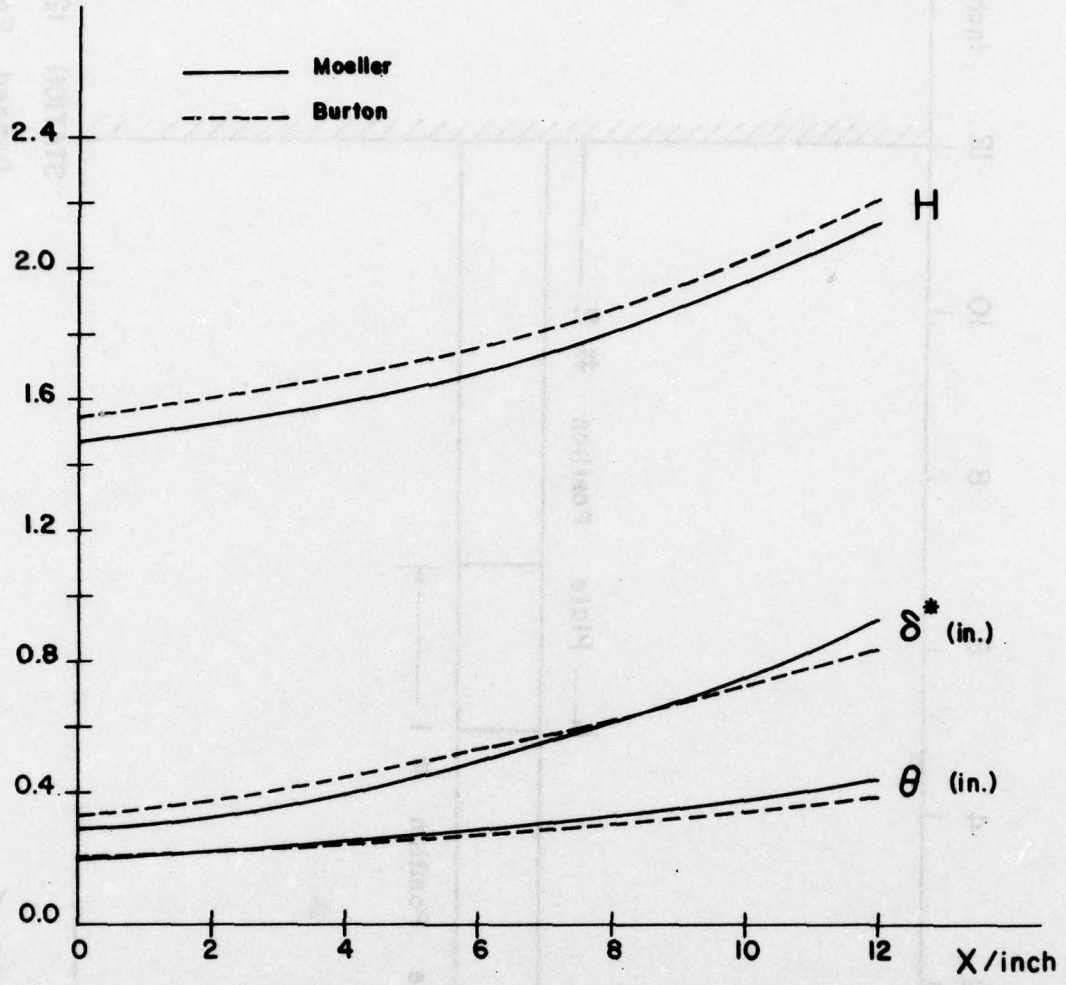

FIGURE 3.6 Mean Boundary Layer Properties for the Adverse Gradient Experiments

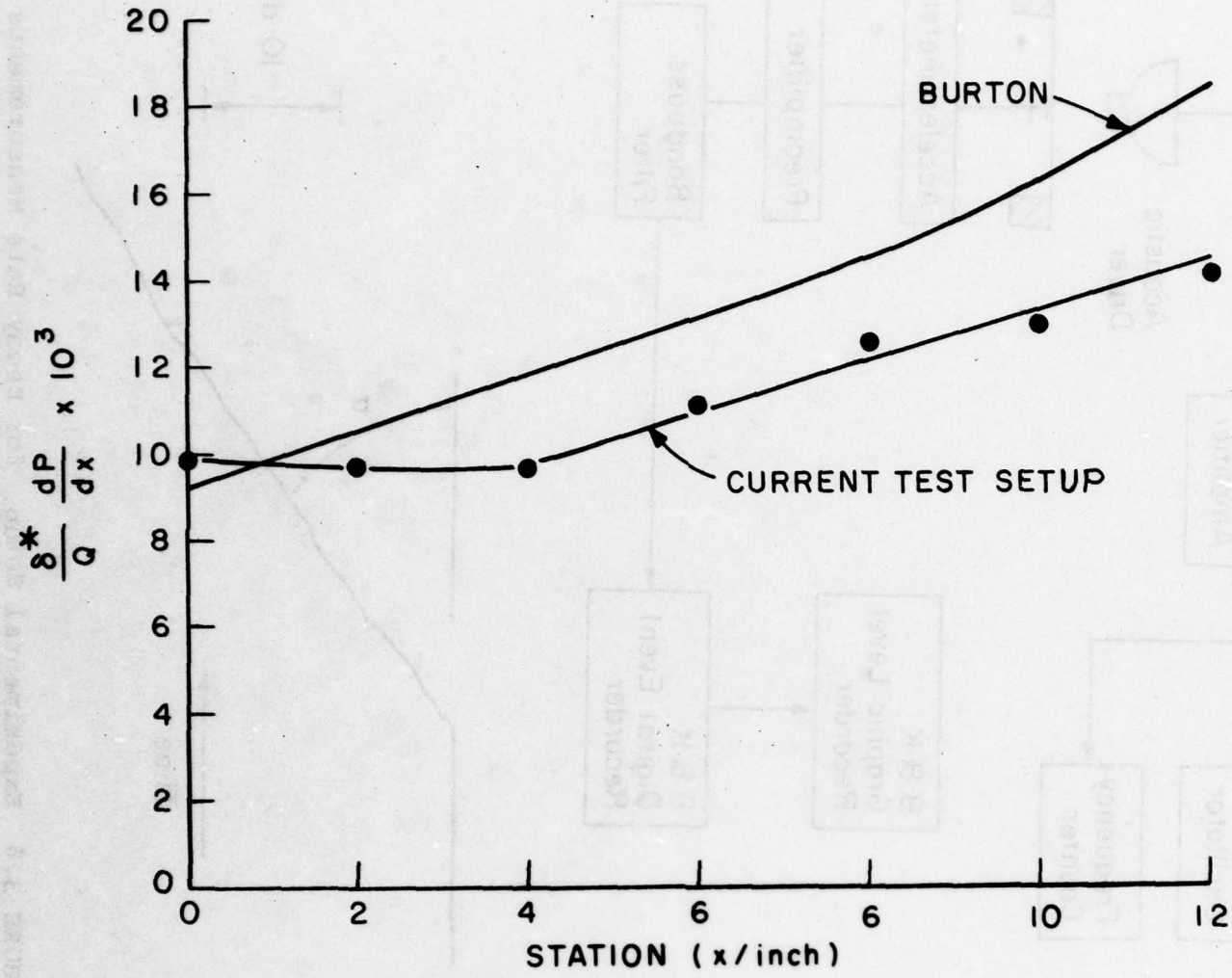

FIGURE 3.7 Nondimensional Pressure Gradient, $\frac{\delta^*}{Q}\frac{dP}{dx}$, for the Adverse Gradient Experiments

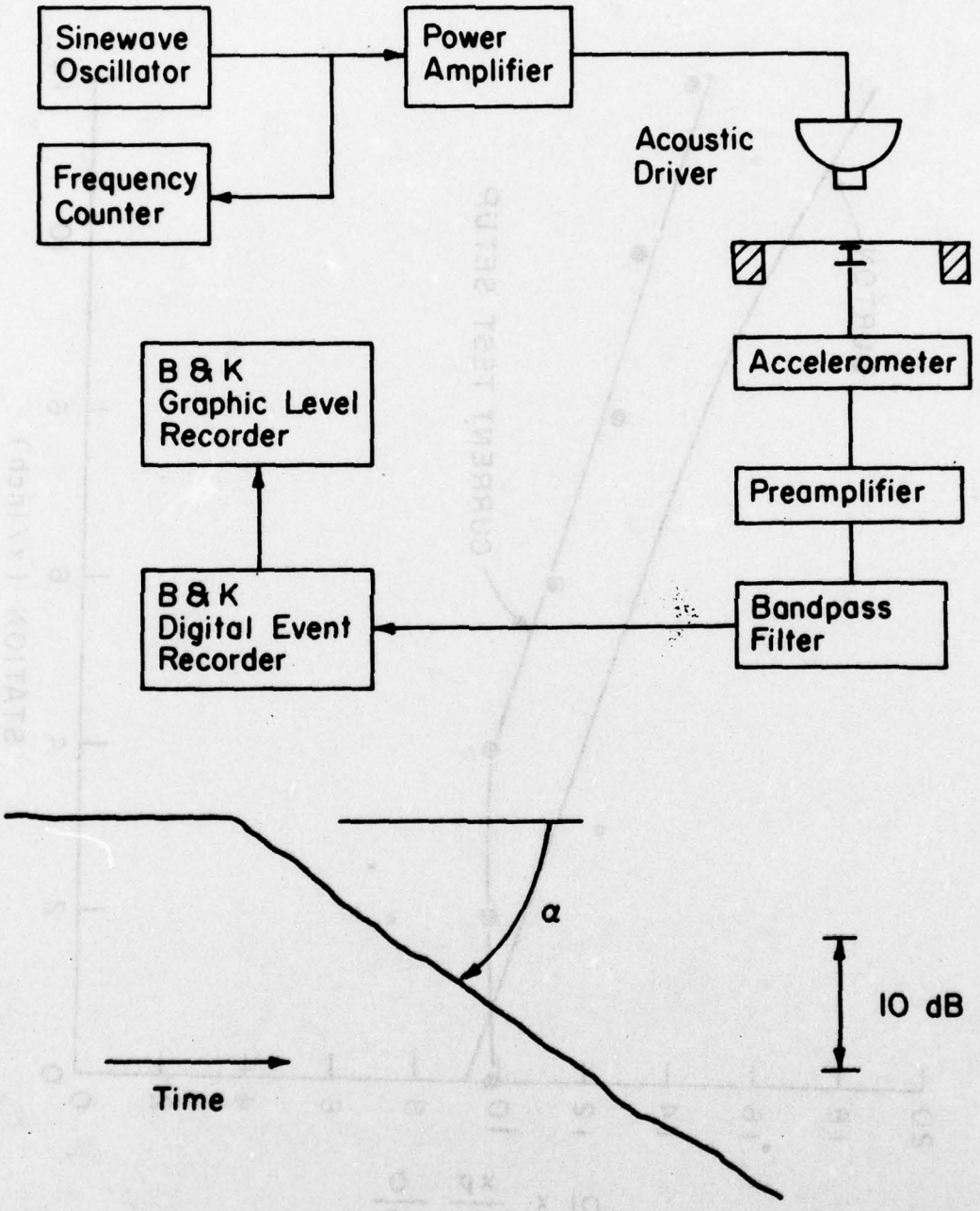

FIGURE 3.8 Experimental Setup for Decay Rate Measurements and Typical RMS Decay Record

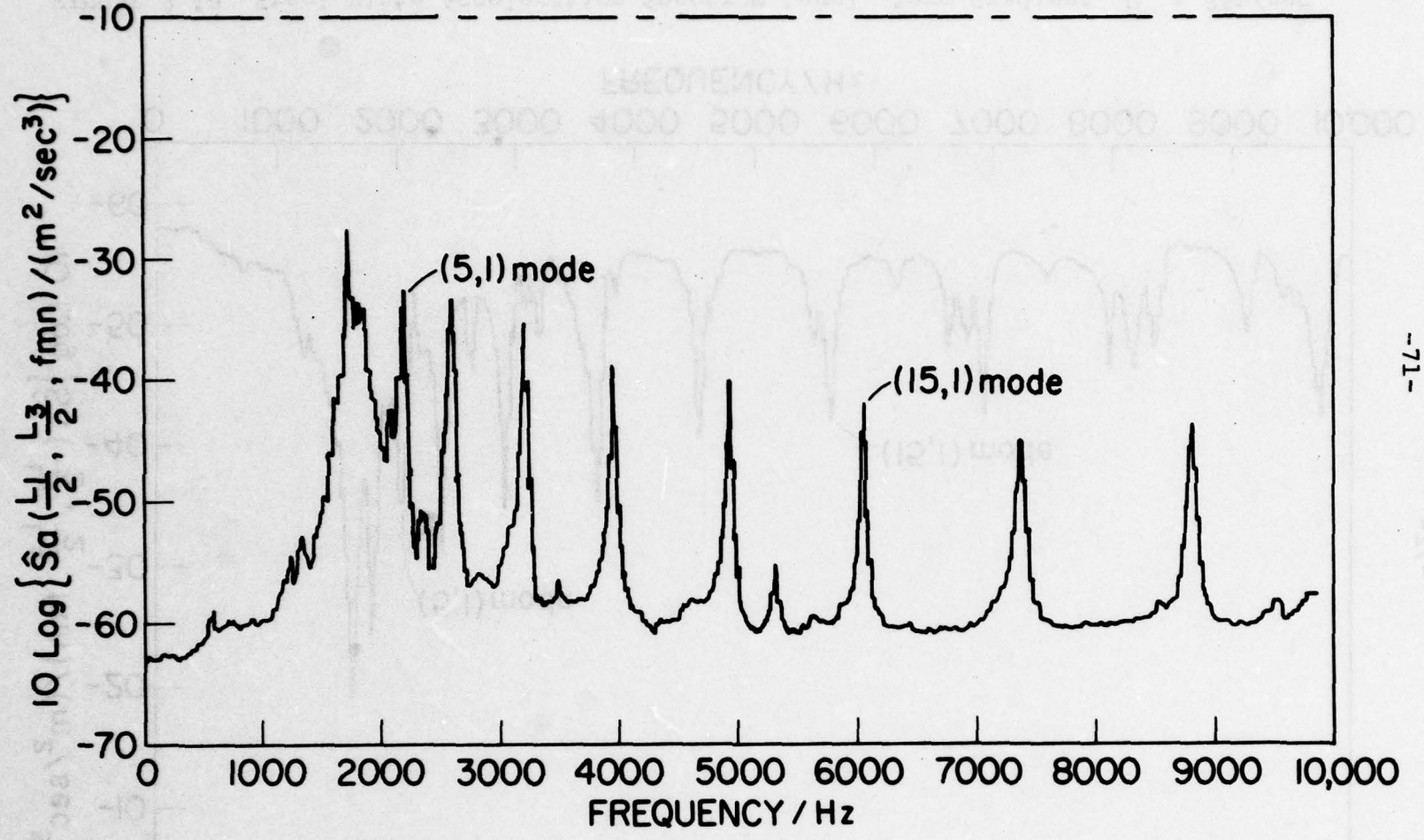

FIGURE 3.9 Brass Plate Acceleration Spectrum Level, Zero Gradient, U_∞ = 35m/sec

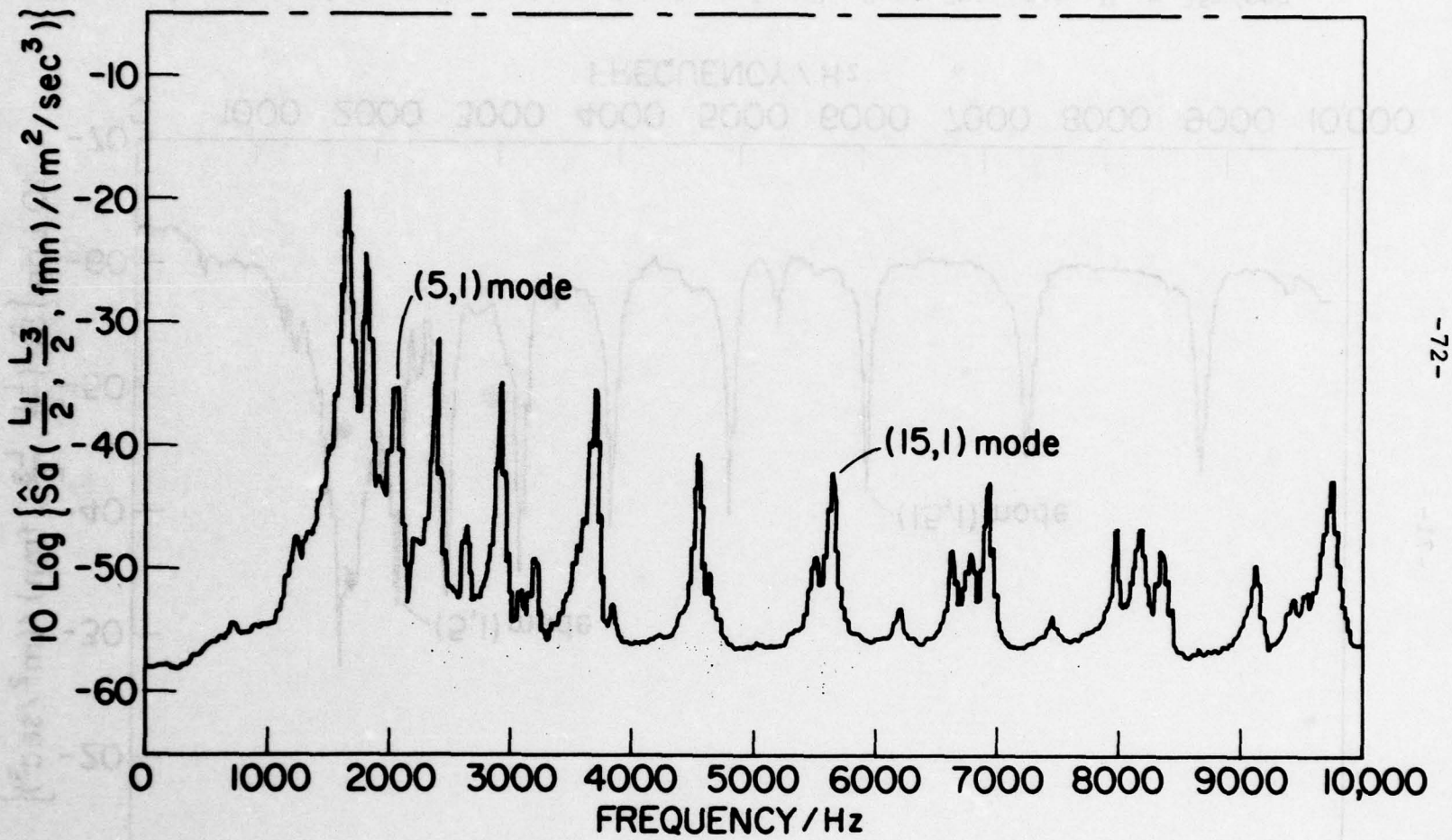

FIGURE 3.10 Steel Plate Acceleration Spectrum Level, Zero Gradient, U_∞ = 35m/sec

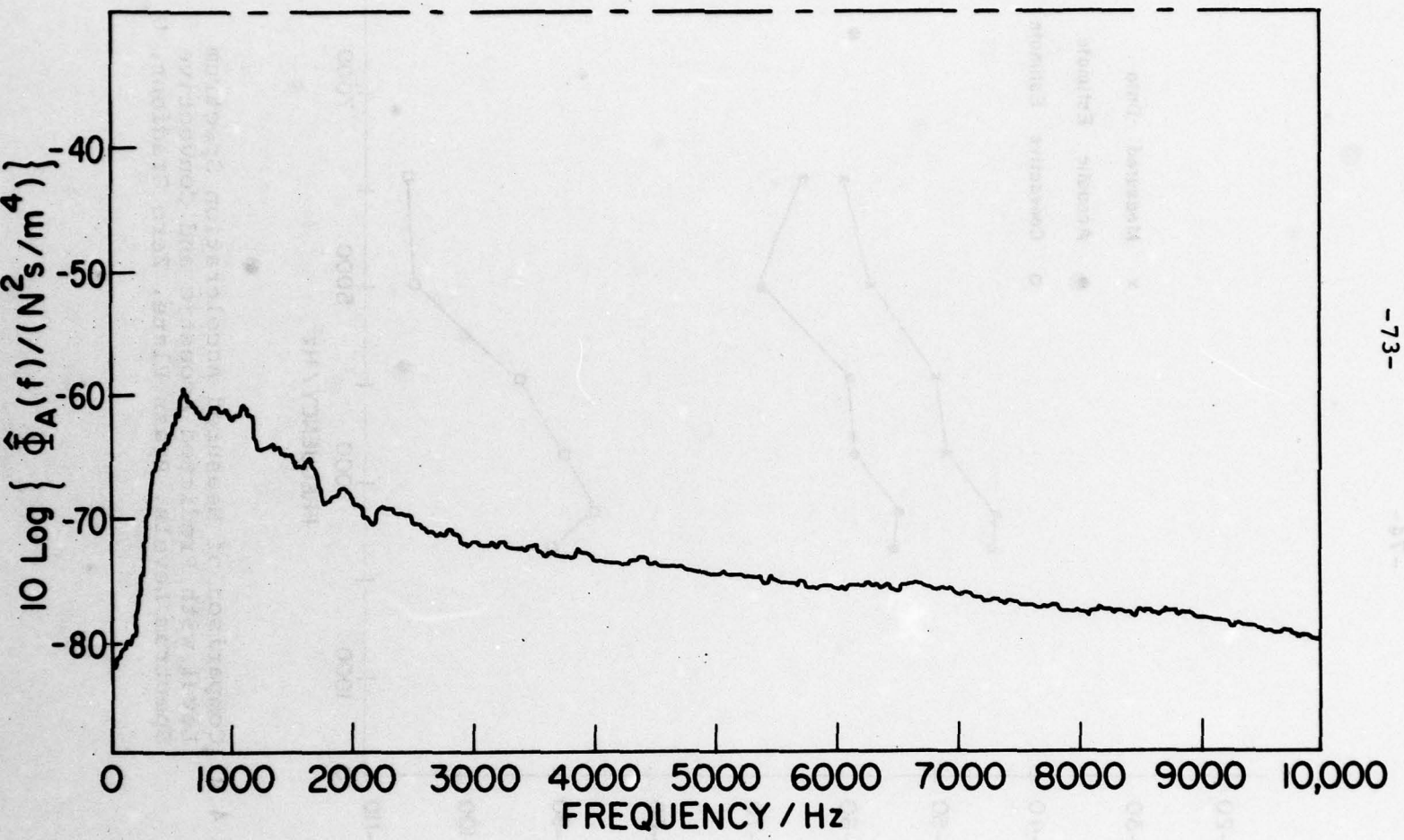

FIGURE 4.1 Typical Acoustic Spectrum Level, Zero Gradient, U_∞ = 35m/sec

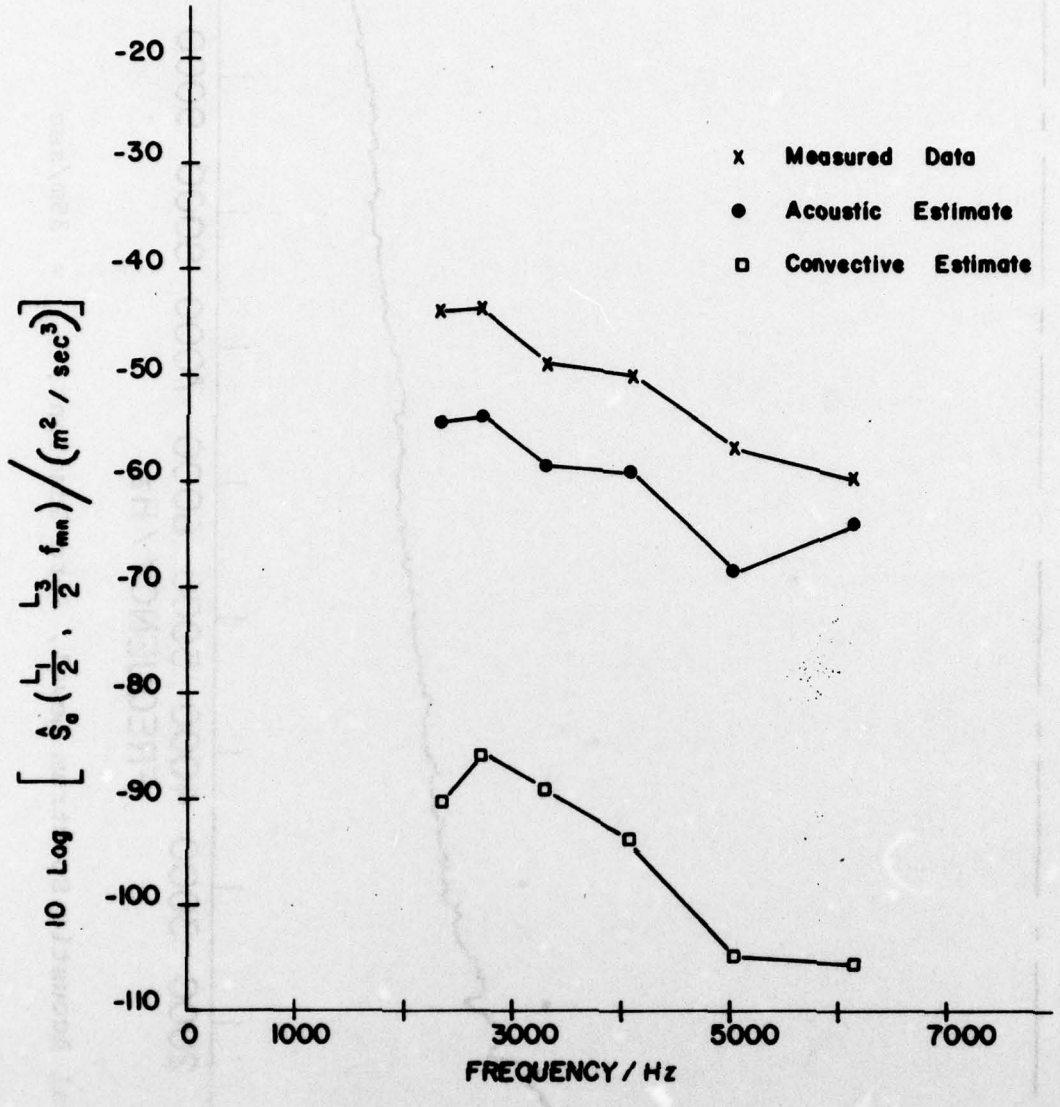

FIGURE 4.2 Comparison of Measured Acceleration Spectrum Level with Predicted Acoustic and Convective Spectrum Levels, Brass Plate, Zero Gradient, U_∞ =20m/sec

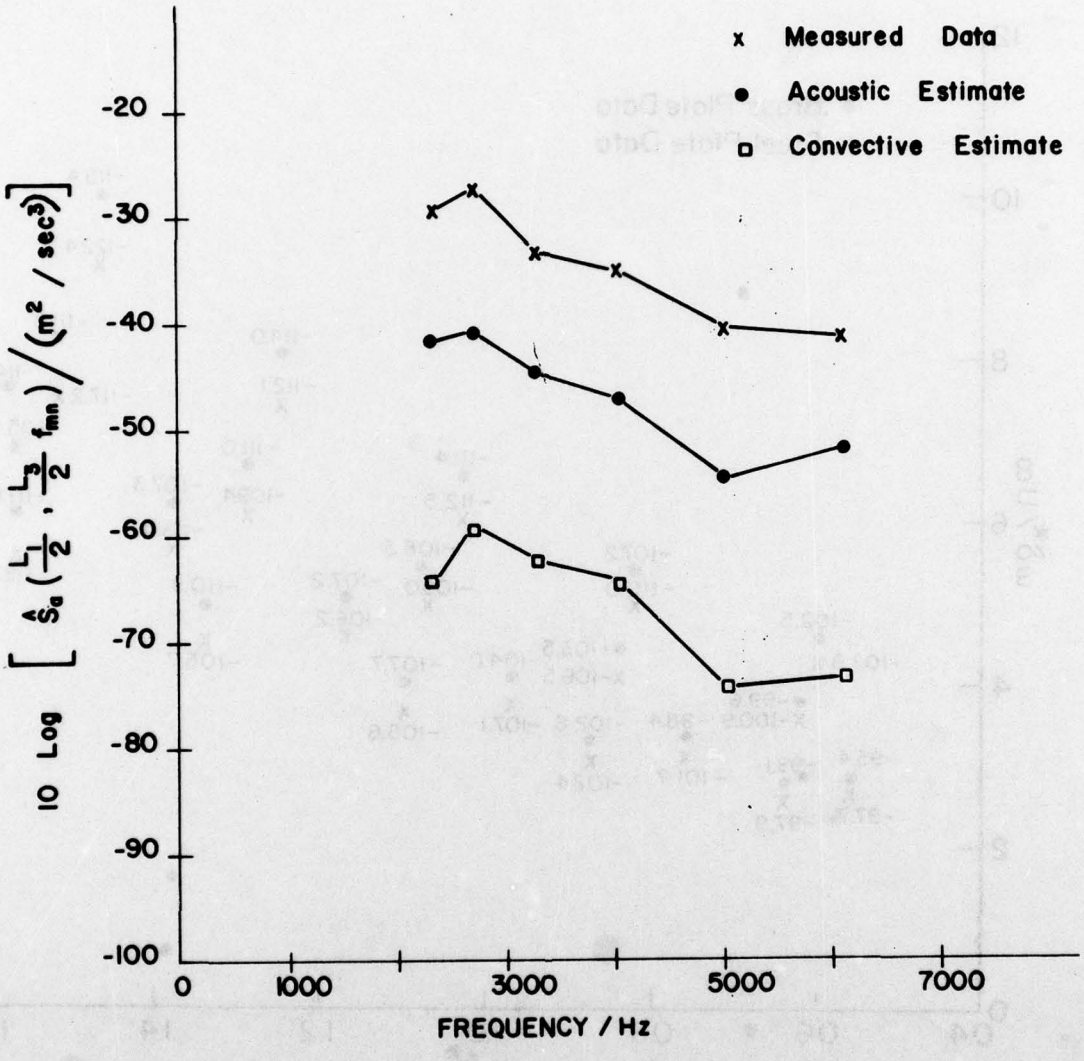

FIGURE 4.3 Comparison of Measured Acceleration Spectrum Level with Predicted Acoustic and Convective Spectrum Levels, Brass Plate, Zero Gradient, U_∞ = 35m/sec

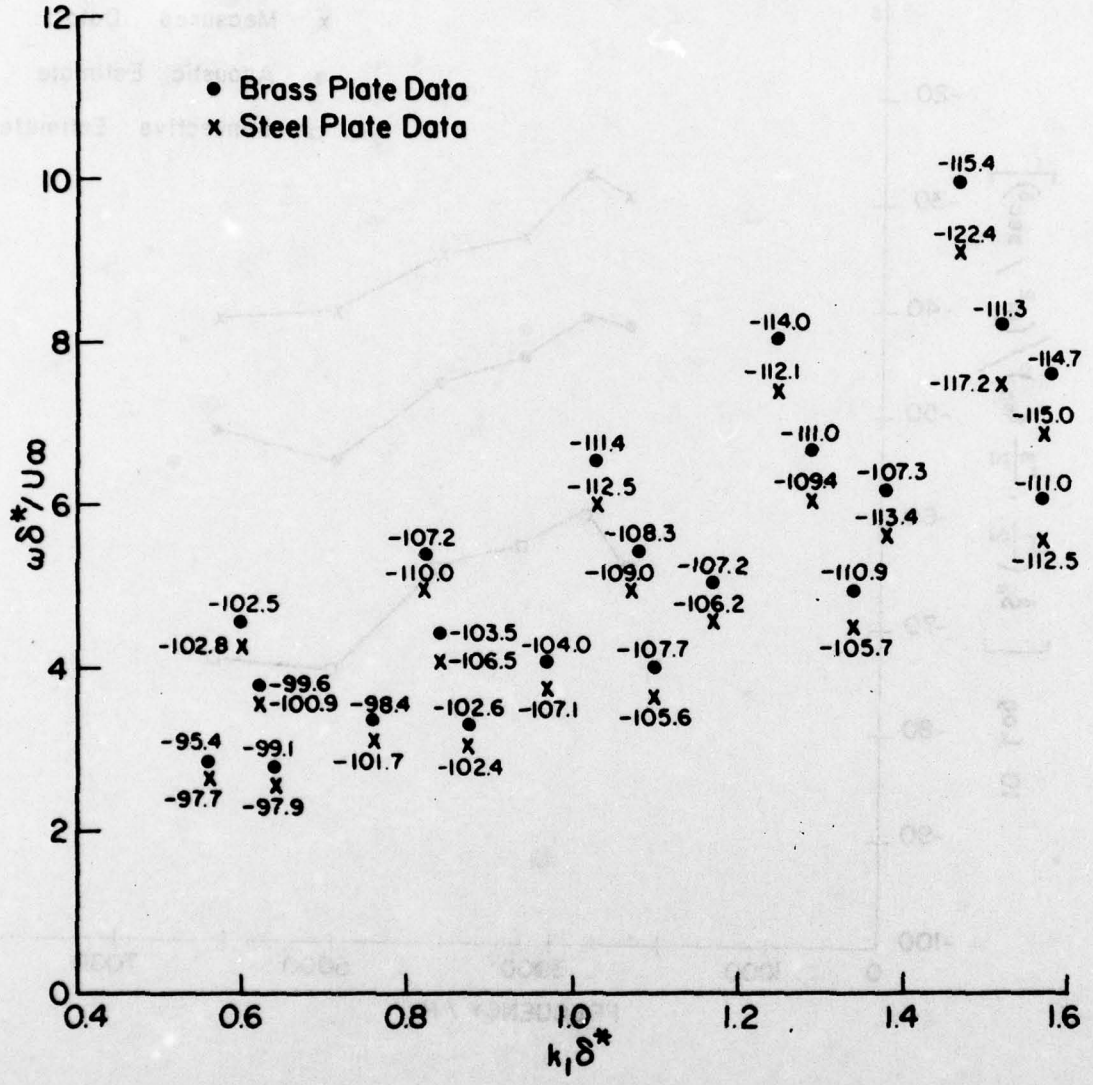

FIGURE 4.4 Location of Low Wavenumber Data in Wavenumber Frequency Space for Zero Gradient, Numbers Indicate Levels of 10 Log$\{P(k_1^*, o, \omega^*)/(q^2\delta^{*3}/U_\infty)\}$

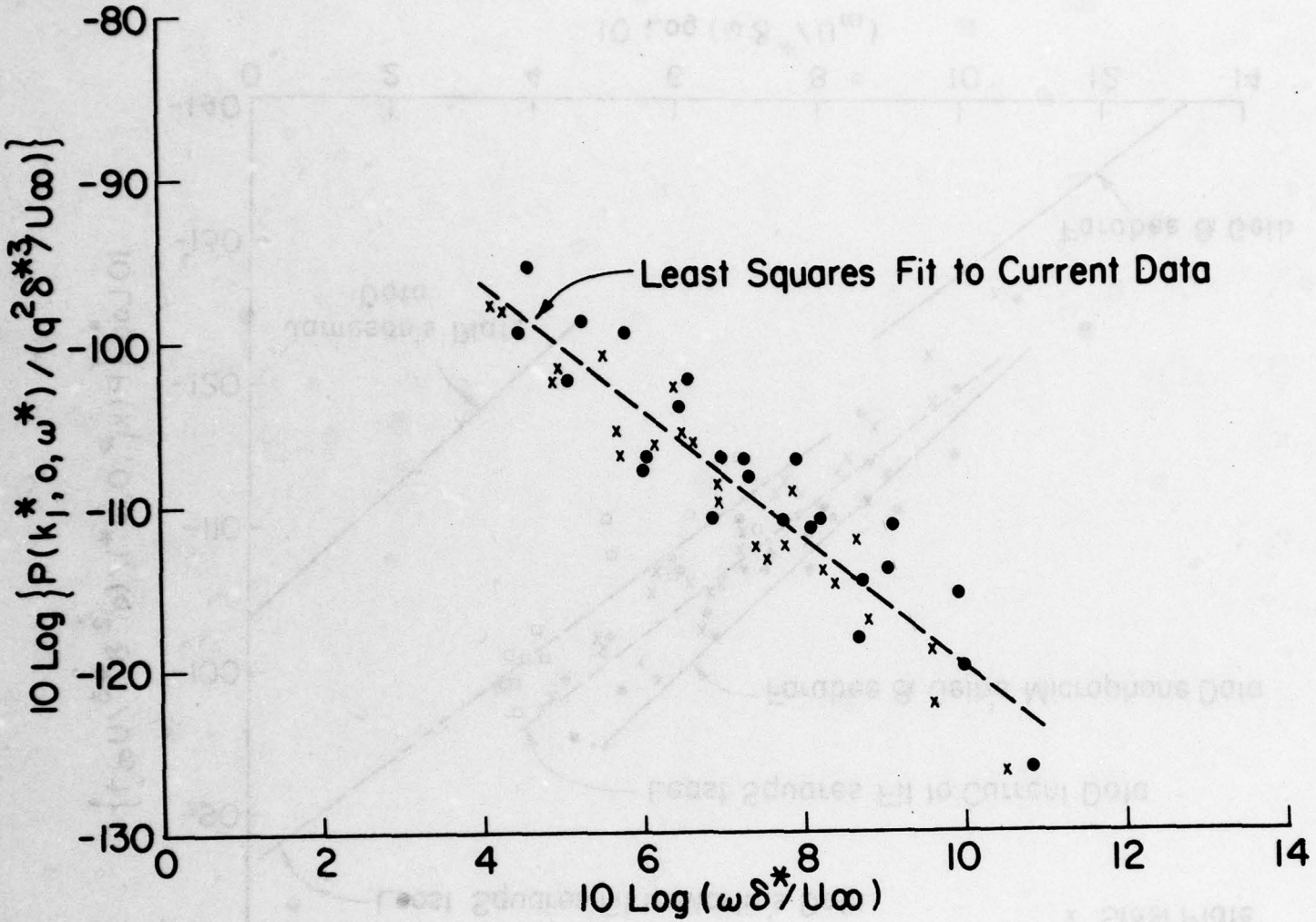

FIGURE 4.5 Measured Low Wavenumber Levels of the Turbulent Boundary Layer Under Zero Gradient

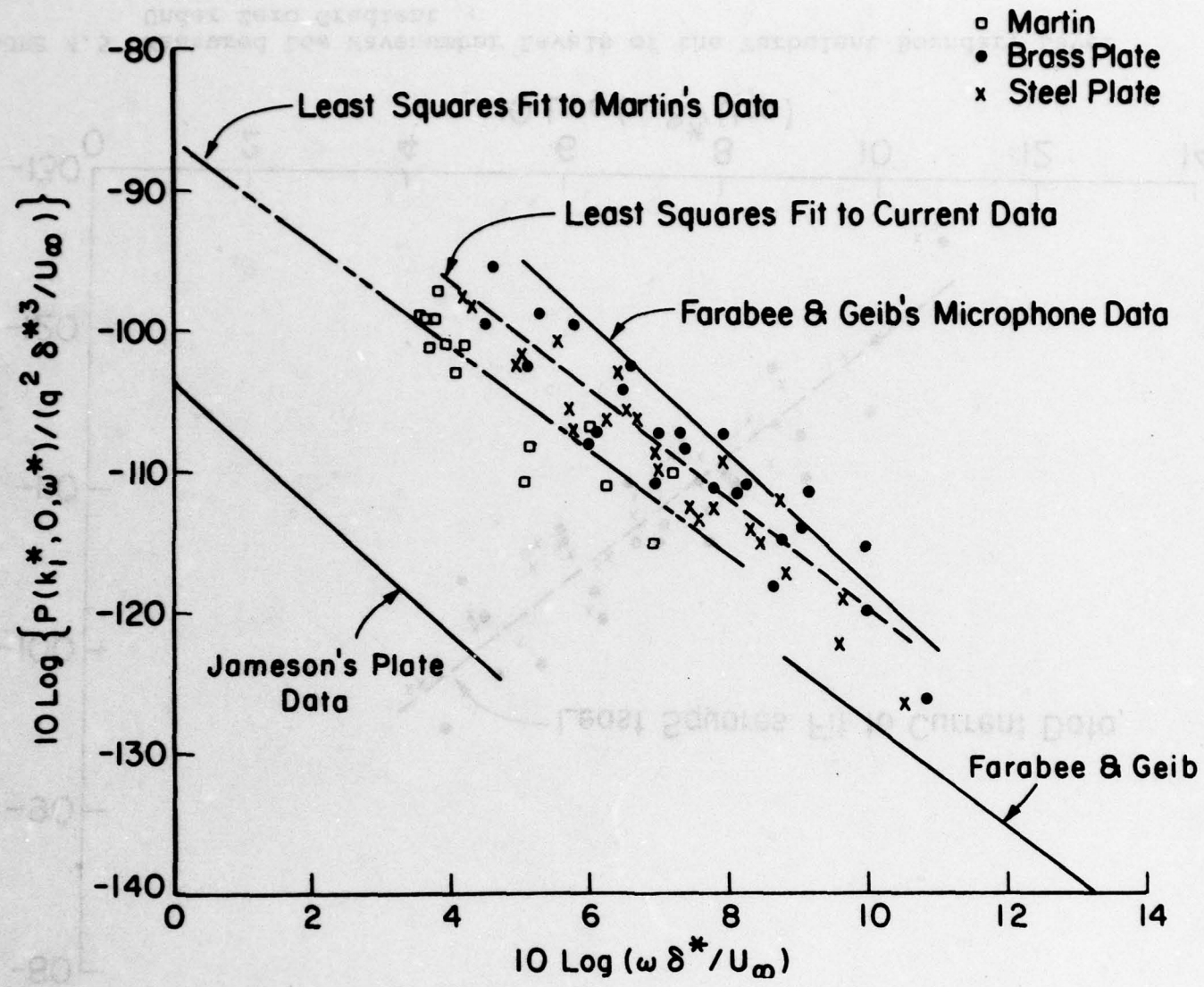

FIGURE 4.6 Comparison of the Measured Low Wavenumber Levels Under Zero Gradient with Other Investigators

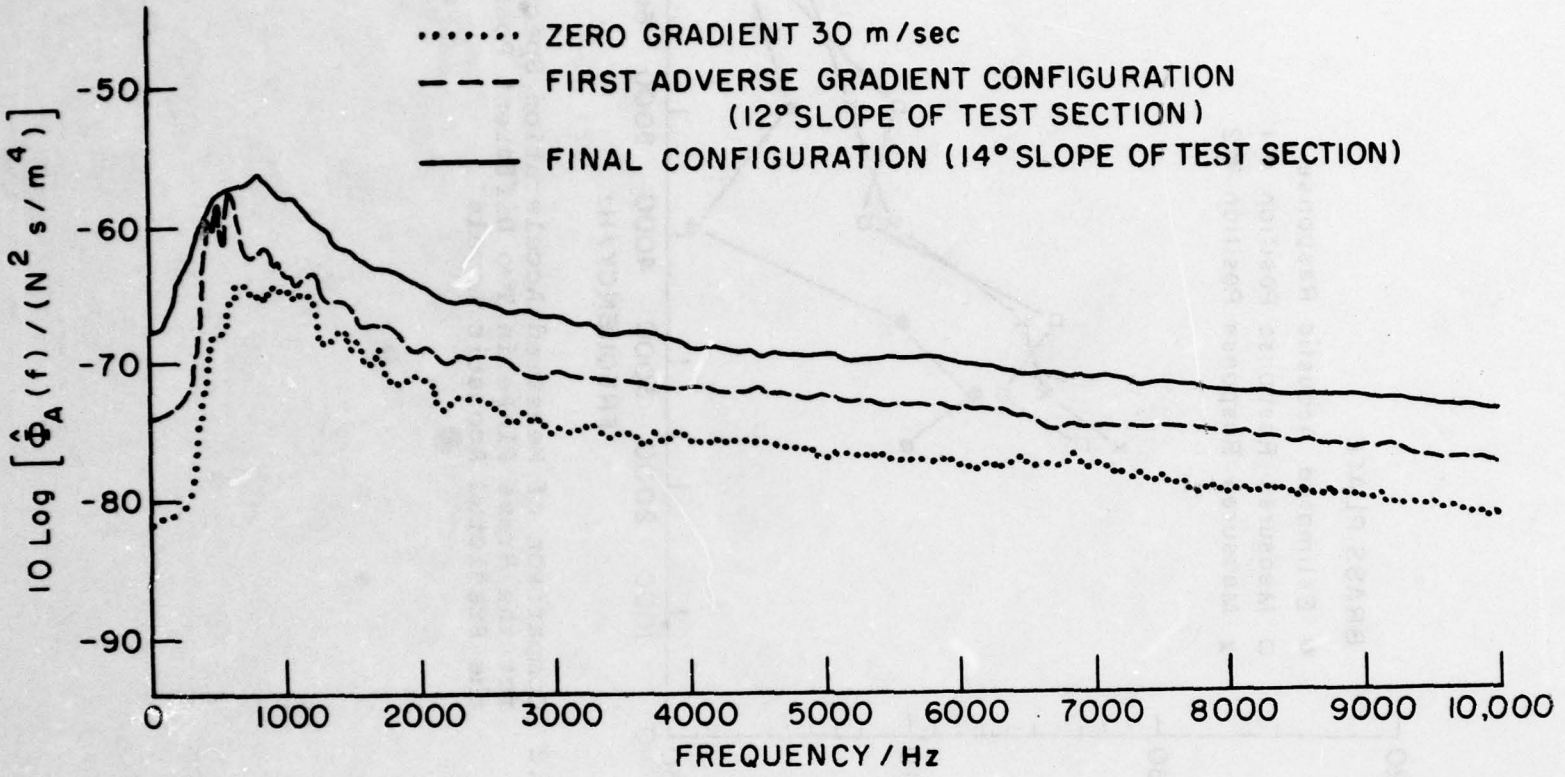

FIGURE 5.1 Acoustic Background Spectrum Levels for Two Adverse Gradient Configurations and a Zero Gradient Configuration at the Same Test Speed

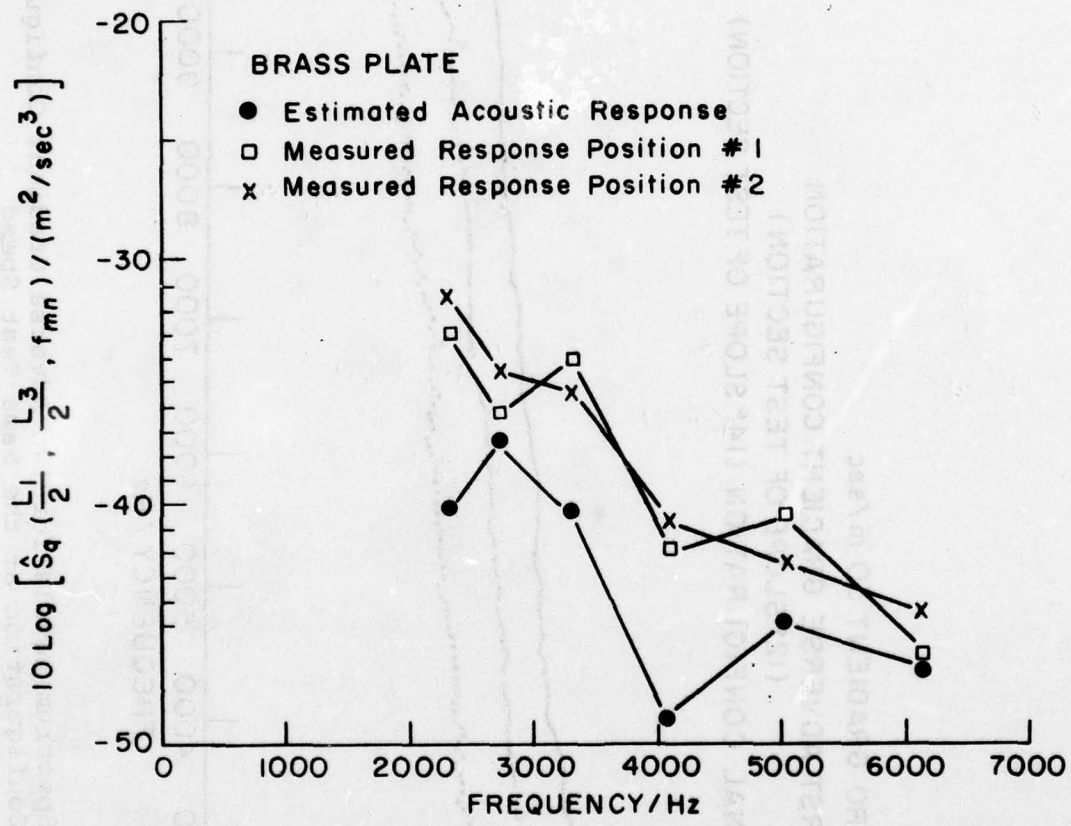

FIGURE 5.2 Comparison of Measured Acceleration Spectrum Levels for the Brass Plate in Two Different Positions with the Predicted Acoustic Levels

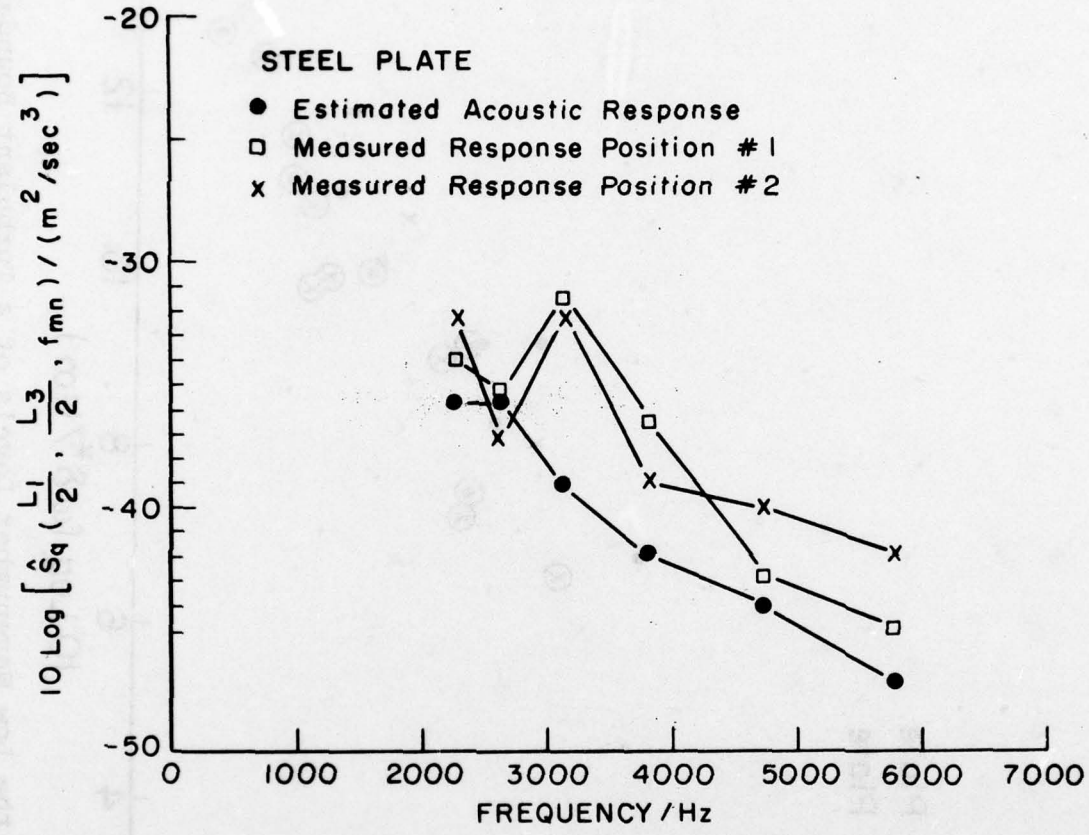

FIGURE 5.3 Comparison of Measured Acceleration Spectrum Levels for the Steel Plate in Two Different Positions with the Predicted Acoustic Spectrum Level

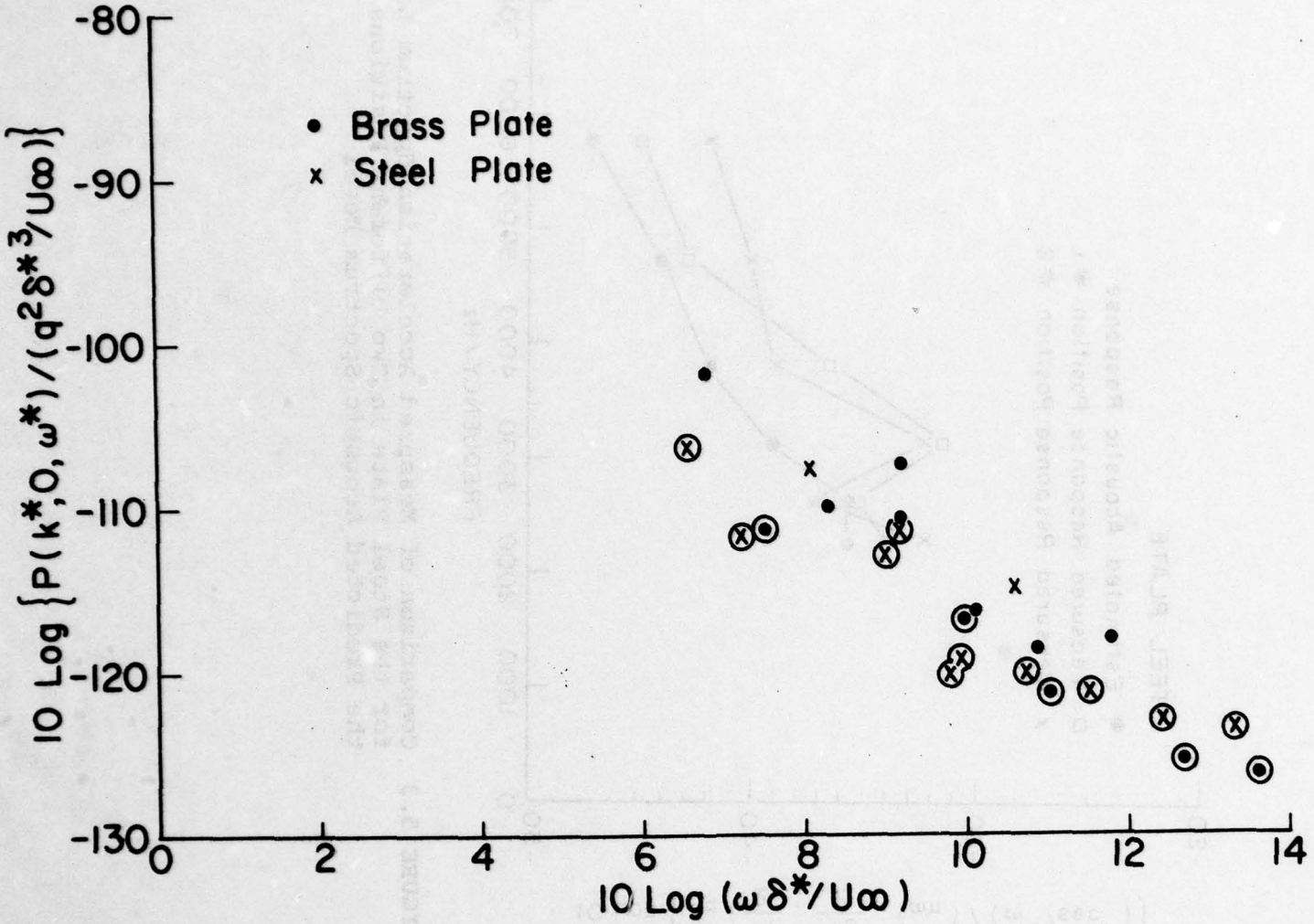

FIGURE 5.4 Measurements of the Low Wavenumber Levels of a Turbulent Boundary Layer Under an Adverse Gradient, Nondimensionalized on Outer Boundary Layer Parameters, The Points Circled May Be Acoustically Contaminated

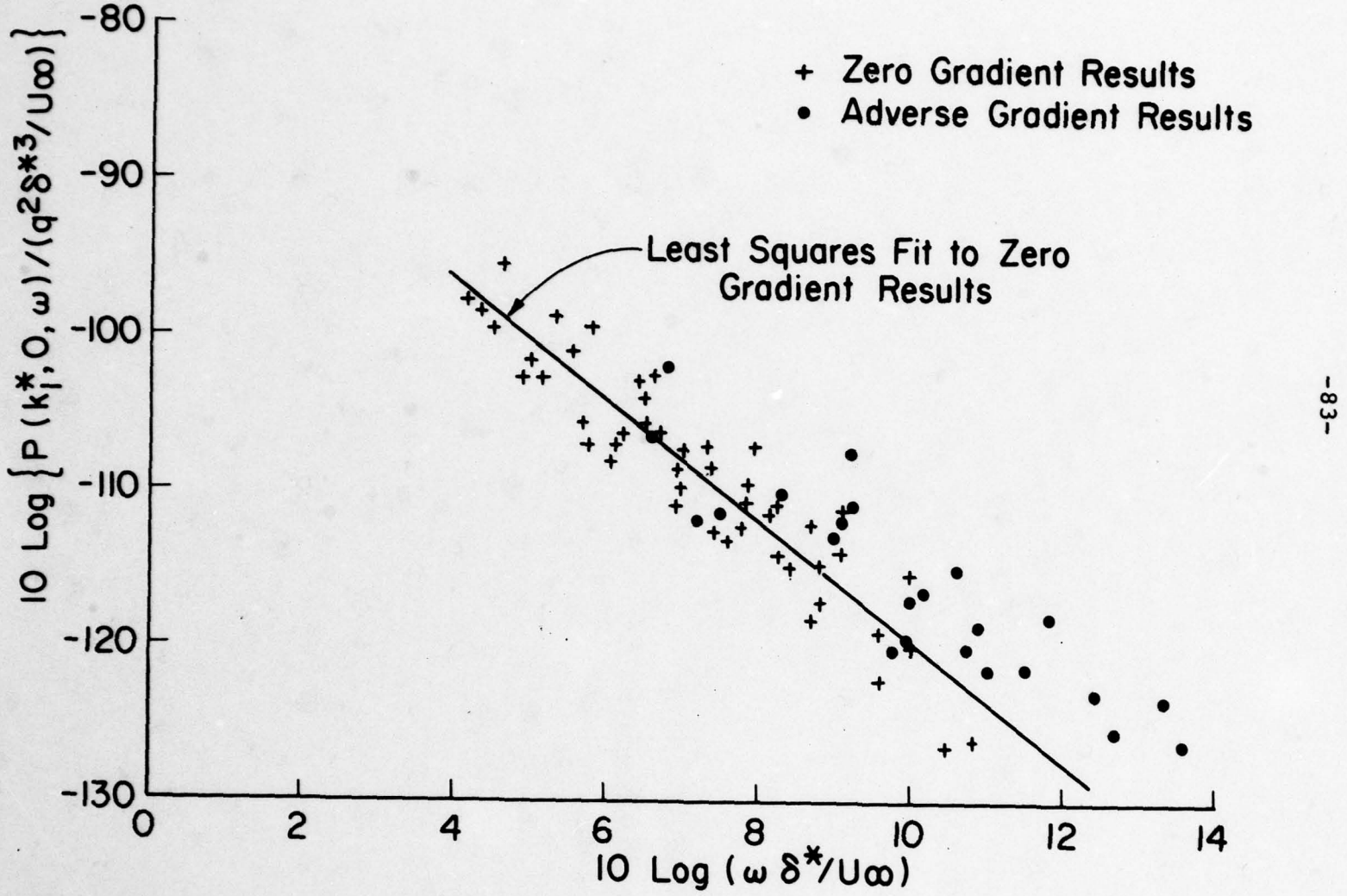

FIGURE 5.5 Comparison of the Low Wavenumber Levels of a Turbulent Boundary Layer Under an Adverse Gradient with the Low Wavenumber Levels of a Turbulent Boundary Layer under a Zero Gradient

REFERENCES

1. Blake, W. K., "Turbulent-Boundary-Layer Wall-Pressure Fluctuations on Smooth and Rough Walls", J. Fluid Mech., 44, pp 637-660, (1970)

2. Burton, T. E., "Wall Pressure Fluctuations at Smooth and Rough Surfaces Under Turbulent Boundary Layers with Favorable and Adverse Pressure Bradients", M.I.T. Acoustics and Vibration Laboratory Report No. 70208-9, (1973)

3. Wills, J. A. B., "Measurements of the Wavenumber/ Phase Velocity Spectrum for Wall Pressure Beneath a Turbulent Boundary Layer", J. Fluid Mech., 45, pp 65-90, (1971)

4. Maidanik, G., and Jorgensen, D. W., "Boundary Wave-Vector Filters for the Study of the Pressure Field in a Turbulent Boundary Layer", J.A.S.A., 42, pp494-501, (1967)

5. Blake, W. K., and Chase, D. M., "Wavenumber-Frequency Spectra of Turbulent-Boundary-Layer Pressure Measured by Microphone Arrays", J.A.S.A.,89, pp 862-877, (1971)

6. Jameson, P. W., "Measurement of Low-Wavenumber Component of Turbulent Boundary Layer Wall Pressure Spectrum", Bolt Beranck and Newman Report No. 1937, (1970)

7. Farabee, T. M. and Geib, F. E. Jr., "Measurement of Boundary Layer Pressure Fields with an Array of Pressure Transducers in Subsonic Flow', D.W.T. Naval Ship Research and Developement Center Report No. 76-0031, (1976)

8. Aupperle, F. A., and Lambert R. F., "On the Utilization of a Flexible Beam as a Spatial Filter", J. Sound Vib., 29, pp 259-267, (1977)

9. Martin, N. C., and Leehey, P., "Low Wavenumber Wall Pressure Measurements Using a Rectangular Membrane as a Spatial Filter", J. Sound Vib., 52, pp 95-120, (1977)

10. Jameson, P. W., "Measurement of the Low Wavenumber Component of Turbulent Boundary Layer Pressure Spectral Density", 4th Symposium on Turbulence in Liquids, Univ. of Missouri- Rolla, (September 1975)

11. Martin, N. C., "Wavenumber Filtering by Mechanical Structures". Ph.D. Thesis, Mass. Inst. of Tech., (January 1976)

12. Hanson, C. E., "The Design and Construction of a Low-Noise Low-Turbulence Wind Tunnel", M.I.T. Acoustics and Vibration Laboratory Report No. 79611 - 1 (1969)

13. Leissa, W. W. "Vibration of Plates", NASA SP-160, (1967)

M.I.T., A & V Report 82464-2
Low Wavenumber Levels of Turbulent Boundary Layer Wall Pressure Fluctuations in Zero and Adverse Gradients, by M. Moeller, P. Leehey, and N.C. Martin, September 1977, 87 pgs., illustrated. UNCLASSIFIED

The low wavenumber components of the turbulent boundary layer wavenumber frequency spectrum of wall pressure fluctuations were measured with two flush-mounted rectangular plates having approximately clamped boundary conditions. The plates were designed to provide low wavenumber measurements at higher frequencies and wavenumbers than previous plate experiments in order to provide data comparable with measurements made by Farabee and Geib [7] with an array of flush-mounted microphones. The low wavenumber measurements were made in the M.I.T. low noise low turbulence subsonic wind tunnel under zero and adverse pressure gradient conditions. When nondimensionalized on outer boundary layer variables the adverse pressure gradient data do not exhibit increased levels from those of the zero pressure gradient data. The zero pressure gradient data are in good agreement with the levels reported by Farabee and Geib [7] for the same nondimensional frequency and wavenumber range.

Turbulent Boundary Layers
Low Wavenumber Levels
Flow Induced Vibration

M.I.T., A & V Report 82464-2
Low Wavenumber Levels of Turbulent Boundary Layer Wall Pressure Fluctuations in Zero and Adverse Gradients, by M. Moeller, P. Leehey, and N.C. Martin, September 1977, 87 pgs., illustrated. UNCLASSIFIED

The low wavenumber components of the turbulent boundary layer wavenumber were spectrum of wall pressure fluctuations were measured with two flush-mounted rectangular plates having approximately clamped boundary conditions. The plates were designed to provide low wavenumber measurements at higher frequencies and wavenumbers than previous plate experiments in order to provide data comparable with measurements made by Farabee and Geib [7] with an array of flush-mounted microphones. The low wavenumber measurements were made in the M.I.T. low noise low turbulent subsonic wind tunnel under zero and adverse pressure gradient conditions. When nondimensionalized on outer boundary layer variables the adverse pressure gradient data do not exhibit increased levels from those of the zero pressure gradient data. The zero pressure gradient data are in good agreement with the levels reported by Farabee and Geib [7] for the same nondimensional frequency and wavenumber range.

Turbulent Boundary Layers
Low Wavenumber Levels
Flow Induced Vibration

M.I.T., A & V Report 82464-2
Low Wavenumber Levels of Turbulent Boundary Layer Wall Pressure Fluctuations in Zero and Adverse Gradients, by M. Moeller, P. Leehey, and N.C. Martin, September 1977, 87 pgs., illustrated. UNCLASSIFIED

The low wavenumber components of the turbulent boundary layer wavenumber were spectrum of wall pressure fluctuations were measured with two flush-mounted rectangular plates having approximately clamped boundary conditions. The plates were designed to provide low wavenumber measurements at higher frequencies and wavenumbers than previous plate experiments in order to provide data comparable with measurements made by Farabee and Geib [7] with an array of flush-mounted mitrophones. The low wavenumber measurements were made in the M.I.T. low noise low turbulent subsonic wind tunnel under zero and adverse pressure gradient conditions. When nondimensionalized on outer boundary layer variables the adverse pressure gradient data do not exhibit increased levels from those of the zero pressure gradient data. The zero pressure gradient data are in good agreement with the levels reported by Farabee and Geib [7] for the same nondimensional frequency and wavenumber range.

Turbulent Boundary Layers
Low Wavenumber Levels
Flow Induced Vibration

M.I.T., A & V Report 82464-2
Low Wavenumber Levels of Turbulent Boundary Layer Wall Pressure Fluctuations in Zero and Adverse Gradients, by M. Moeller, P. Leehey, and N.C. Martin, September 1977, 87 pgs., illustrated. UNCLASSIFIED

The low wavenumber components of the turbulent boundary layer wavenumber frequency spectrum of wall pressure fluctuations were measured with two flush-mounted rectangular plates having approximately clamped boundary conditions. The plates were designed to provide low wavenumber measurements at higher frequencies and wavenumbers than previous plate experiments in order to provide data comparable with measurements made by Farabee and Geib [7] with an array of flush-mounted microphones. The low wavenumber measurements were made in the M.I.T. low noise low turbulence subsonic wind tunnel under zero and adverse pressure gradient conditions. When nondimensionalized on outer boundary layer variables the adverse pressure gradient data do not exhibit increased levels from those of the zero pressure gradient data. The zero pressure gradient data are in good agreement with the levels reported by Farabee and Geib [7] for the same nondimensional frequency and wavenumber range.

Turbulent Boundary Layers
Low Wavenumber Levels
Flow Induced Vibration